Neurotherapeutics (2023) 20:1081–1108
https://doi.org/10.1007/s13311-023-01356-6

ORIGINAL ARTICLE

# Ferulic Acid Improves Synaptic Plasticity and Cognitive Impairments by Alleviating the PP2B/DARPP-32/PP1 Axis-Mediated STEP Increase and Aβ Burden in Alzheimer's Disease

**Yacoubou Abdoul Razak Mahaman[1,2,3] · Fang Huang[3] · Maibouge Tanko Mahamane Salissou[3,4] · Mohamed Bassirou Moukeila Yacouba[5] · Jian-Zhi Wang[1,3,6] · Rong Liu[3] · Bin Zhang[3] · Hong-Lian Li[3] · Feiqi Zhu[2] · Xiaochuan Wang[1,3,6,7]**

Accepted: 14 February 2023 / Published online: 20 April 2023


## Abstract

The burden of Alzheimer's disease, the most prevalent neurodegenerative disease, is increasing exponentially due to the increase in the elderly population worldwide. Synaptic plasticity is the basis of learning and memory, but it is impaired in AD. Uncovering the disease's underlying molecular pathogenic mechanisms involving synaptic plasticity could lead to the identification of targets for better disease management. Using primary neurons treated with Aβ and APP/PS1 animal models, we evaluated the effect of the phenolic compound ferulic acid (FA) on synaptic dysregulations. Aβ led to synaptic plasticity and cognitive impairments by increasing STEP activity and decreasing the phosphorylation of the GluN2B subunit of NMDA receptors, as well as decreasing other synaptic proteins, including PSD-95 and synapsin1. Interestingly, FA attenuated the Aβ-upregulated intracellular calcium and thus resulted in a decrease in PP2B-induced activation of DARPP-32, inhibiting PP1. This cascade event maintained STEP in its inactive state, thereby preventing the loss of GluN2B phosphorylation. This was accompanied by an increase in PSD-95 and synapsin1, improved LTP, and a decreased Aβ load, together leading to improved behavioral and cognitive functions in APP/PS1 mice treated with FA. This study provides insight into the potential use of FA as a therapeutic strategy in AD.

**Keywords** Alzheimer's disease · PP2B/DARPP-32/PP1 axis · Synapses · Increased intracellular calcium · Ferulic acid · Cognitive impairment

## Introduction

Synaptic plasticity is the basic process that leads to memory formation, and NMDA receptors (NMDARs) are central to synaptic plasticity and thus learning and memory [1]. Accumulating evidence suggests that the NMDAR subunit composition (GluN2A or GluN2B), as well as the localization (synaptic or extrasynaptic), are critical for synaptic plasticity [2, 3]. The intracellular phosphatase striatal-enriched protein tyrosine phosphatase (STEP) is the main regulator of the phosphorylation of the NMDA and AMPA receptor subunits GluN2B and GluA2, respectively [4–7]. STEP is

Yacoubou Abdoul Razak Mahaman, Fang Huang, and Hong-Lian Li contributed equally to this work.

✉ Feiqi Zhu
zfqzsu2004@aliyun.com

✉ Xiaochuan Wang
wxch@mails.tjmu.edu.cn

1 Coinnovation Center of Neuroregeneration, Nantong University, Nantong, JS 226001, China

2 Cognitive Impairment Ward of the Neurology Department, The Third Affiliated Hospital of Shenzhen University, 47 Youyi Rd., Shenzhen, Guangdong Province 518001, China

3 Department of Pathophysiology, School of Basic Medicine, Key Laboratory of Education Ministry/Huibei Province of China for Neurological Disorders, Tongji Medical College, Huazhong University of Science and Technology, Wuhan 430030, China

4 College of Health, Natural and Agriculture Sciences, Africa University, Mutare, Zimbabwe

5 Department of Anesthesiology, Zhongnan Hospital of Wuhan University, Wuhan, Hubei 430071, China

6 Department of Pathology and Pathophysiology, School of Medicine, Jianghan University, Wuhan 430056, China

7 Shenzhen Huazhong University of Science and Technology Research Institute, Shenzhen 518000, China

encoded by the PTPN5 gene, widely distributed throughout the central nervous system (CNS) except in the cerebellum [8], and has four spliced variants (STEP61, STEP46, STEP38, and STEP20), of which STEP61 (here referred to as STEP unless stated otherwise) is the only variant expressed in the cortex and hippocampus [9, 10]. A fifth variant of STEP, a proteolytic cleavage product of calpain, has also been reported [11]. STEP is implicated in several neurodegenerative disorders, including Alzheimer's disease (AD), Parkinson's disease, Huntington's disease, schizophrenia, fragile X syndrome, and age-related memory decline [4, 12, 13]. AD is currently the most widely prevalent neurodegenerative disease affecting global health, deteriorating behavior, and cognitive capacities in aged individuals [14, 15]. It is a major public health problem in modern society that will exponentially increase in the coming years unless therapeutic strategies become available. The histopathology of AD is marked by extracellular senile plaques and intracellular neurofibrillary tangles (NFTs), which are predominantly composed of amyloid-β (Aβ) peptides and hyperphosphorylated tau, respectively. Aβ peptides are believed to be the trigger of AD pathogenesis and result from the proteolysis of amyloid precursor protein (APP) by two proteases, beta APP cleaving enzyme 1 (BACE1), also called β-secretase, and γ-secretase [16–18]. Clinically, age-dependent synapse loss and memory impairments are the most common characteristics of AD patients [19] as well as many AD animal models [20]. This might be because synapses are believed to be the memory storage sites and thus are the ultimate final targets for different molecular assaults, such as Aβ or high intracellular calcium influx in neurodegenerative diseases such as AD. Moreover, synaptic dysfunction correlates with the degree of cognitive decline in AD patients and transgenic mice with Aβ toxicity [19]. The failure of many of the drug discovery and development strategies based on tau and Aβ [21, 22] has inspired therapeutic strategy interest in multitarget-directed ligand approaches such as disease-modifying therapies (DMTs), which slow the progression of dementia symptoms, as supported by results from a survey that indicated that synaptic plasticity/neuroprotection agents in phase 3 and phase 2 clinical trials have reached up to 23.5 and 27.3% of DMT, respectively [23].

It has been reported that a decreased concentration of GluN2B and PSD-95, impaired LTP, and decreased NMDA and AMPA receptor currents in the hippocampal CA1 region occurred in transgenic AD mice [24]. STEP not only dephosphorylates GluN2B and GluA2 but also is responsible for the dephosphorylation of the synapse-related kinases Fyn, Pyk2, and ERK1/2 and is reported to be increased in postmortem AD patients and several AD mouse models, such as Tg2576, J20, APP/PS1, and 3×TG mice [4, 13, 25]. Consistently, Aβ treatment was found to induce the endocytosis of NMDARs following STEP dephosphorylation [12]. NMDA receptors are involved in the structural regulation of spines, suggesting that STEP-mediated downregulation of NMDA receptors may contribute to the loss of synaptic density in AD. The increased STEP in AD seems to be the consequence of Aβ-induced dysregulation of the ubiquitin–proteasome system (UPS) and the activation of α7 nicotinic acetylcholine receptors (α7nAChRs) [26–28]. These subsequently lead to the buildup of STEP and increased calcium influx, resulting in the activation of calcineurin (protein phosphatase 2B (PP2B)). The active PP2B subsequently dephosphorylates (inactivates) DARPP-32, the inhibitor of protein phosphatase 1 (PP1), thereby activating PP1, which then dephosphorylates (activates) STEP [25]. Calcium homeostasis disturbances play a critical role in AD by activating CaMKII [29], decreasing PP2A, increasing GSK3β activities [30], and increasing BACE1 activity via cyclin-dependent kinase 5 (CDK5) activation by calpain [31, 32]. Together, these effects lead to tau hyperphosphorylation and Aβ production, resulting in synaptic and cognitive impairments. Interestingly, the pharmacological inhibition [33] and the genetic knockdown [13] of STEP were able to ameliorate cognitive dysfunction and hippocampal memory loss in the 3×Tg-AD mouse model and restore the Tyr1472 phosphorylation of GluN2B in neuronal cultures [33].

The phenolic compound ferulic acid (FA), found in many foods, including fruits, vegetables, and cereals [34], possesses a wide range of biological functions, such as antioxidant, anti-inflammatory, anticarcinogenic, antiviral, cardioprotective, and hepatoprotective functions [35–40], and was found to improve Aβ-induced damage in both cell culture and animal models [34, 35, 37, 41–43]. For example, long-term administration of FA was able to protect mice against Aβ-induced learning and memory impairments and neurons from Aβ-induced oxidative stress and neurotoxicity [44] and to activate protective genes and proteins in regions of the brain involved in memory. A recent study revealed that FA could prevent the decrease in the density and diameter of hippocampal capillaries, resulting in decreased Aβ plaque deposition [45]. However, the molecular mechanisms whereby FA improves cognition are not completely clear. Interestingly, FA could mediate the inhibition of $Ca^{2+}$-dependent glutamate release in synaptosomes by chelating extracellular $Ca^{2+}$ ions and suppressing the depolarization-induced increase in cytosolic free $Ca^{2+}$ concentration by blocking N-type and P/Q-type $Ca^{2+}$ channels [46]. FA has a relatively low molecular weight; therefore, it is easily cell-permeable, absorbable via the stomach mucosa, bioavailable, and can be metabolized in the liver [47]. In rats, FA can be observed in the plasma only 5 min following oral administration, and both free and conjugated FA can be distributed via the systemic circulation into peripheral

tissues [48, 49]. Although it has a negative charge at physiological pH, FA can readily cross the blood–brain barrier following peripheral administration in rodents [50]. A recent study also showed that transdermal administration [51] or conjugation [52] might increase FA bioavailability, while its combination with other compounds might improve its efficacy [35, 37]. In this study, we investigated the molecular mechanism whereby FA improves learning and memory in AD and reported that FA leads to a decrease in STEP by modulating the calcium-related PP2B/DARPP-32/PP1 axis and by alleviating Aβ burden. Together, these effects improved synaptic plasticity and cognitive impairments in the APP/PS1 mouse model of AD.

## Methods

### Primary Neuron Culture

Primary hippocampal neurons were prepared from 16- to 18-day-old pregnant mice. The mice were deeply anesthetized, the embryos were removed, their brains were dissected on ice, and the hippocampi were sliced into small pieces in Hanks' balanced salt solution and digested with trypsin/EDTA for 15 min at 37 °C with shaking every 5 min. The digestion was terminated by the addition of an equal amount of neuronal plating medium (10% fetal bovine serum in DMEM/F12). The tissue was triturated with plating medium, and the cell suspension was passed through a 40-μm filter and plated in a 6-well cell culture plate coated with poly D-lysine. The neurons were incubated in a humidified incubator at 37 °C for 4–6 h with 5% $CO_2$. Then, the medium was replaced with maintenance medium [neurobasal medium supplemented with 2% B27, 1% GlutaMAX, and 1% penicillin (50 U/mL) and streptomycin (50 μg/mL), all from Gibco]. Half of the medium was changed every 3 days with fresh maintenance medium. For Aβ treatment, human Aβ42 peptides (Chinapeptides, Shanghai, China) were first dissolved in DMSO and then in DMEM-high medium at a concentration of 200 μM and incubated overnight at 4 °C for oligomerization before use. The solution was sonicated and centrifuged, and then, the Aβ oligomers were added to the cell medium at a final concentration of 2 μM for 48 h. For ferulic acid treatment, FA was dissolved in DMSO and then diluted in maintenance medium, and the neurons were incubated at concentrations of 5 and 10 μM. For PDP3 treatment, PDP3 was dissolved in DMSO and then diluted in maintenance medium, and the neurons were incubated at a concentration of 20 μM for 2 h. FA treatment was performed 2 h before Aβ or PDP3 incubation. All primary neuron treatments were initiated at day in vitro (DIV) 14, and all control wells were treated with DMSO as a vehicle.

### Western Blot Analysis

Primary hippocampal neurons or brain hippocampi were homogenized in RIPA lysis buffer (Beyotime Biotechnology, Shanghai, China) containing a proteinase inhibitor cocktail (200 mM AEBSF, 30 μM aprotinin, 13 mM bestatin, 1.4 mM E64, and 1 mM leupeptin in DMSO, 1:100) and phenylmethanesulfonylfluoride (PMSF) (1:100) (Yeasen Biotech, Shanghai, China). Then, the lysates were boiled for 10 min and ultrasonicated to completely lyse the tissues. After centrifugation (12,000 × rpm, 15 min, 4 °C), the supernatants were collected, and the protein concentration was measured by a BCA kit (Beyotime Biotechnology). Aliquots of the protein samples were mixed with a 4 × loading buffer containing bromophenol blue at a v/v ratio of 4:1. The samples were electrophoresed on an SDS-PAGE gel, and the proteins were transferred to a nitrocellulose (NC) membrane and blocked for 45 min with 5% skim milk in Tris-buffered saline (TBS; Thermo Fisher; BP24711) and 0.1% Tween-20 (Sigma; P2287). The NC membranes were incubated overnight in primary antibodies (Table 1) at the proper dilution at 4 °C. Membranes were then washed three times in TBS with 0.1% Tween-20 for 10 min each, and appropriate secondary antibodies were added. Membranes were incubated for 1 h at room temperature and washed three times in TBS with 0.1% Tween-20, and the blots were visualized with the Odyssey (LICOR Biosciences, Boston, MA, USA). ImageJ software (1.51n, Wayne Rasband, Bethesda, MD, USA) was used to quantify the density of the bands. The original representative gels of all western blot experiments are shown in the supplementary materials as Supplementary Figs. 1, 2, 3, 4, 5, 6, 7, 8, and 9.

### Immunofluorescence

Primary neurons were cultured and treated on coverslips and then fixed in 4% PFA for 15 min at room temperature and washed with PBS 3 times. The primary neurons on the coverslips were permeabilized with 0.3% Triton X-100 for 15 min and then blocked with 5% bovine serum albumin in 0.1% Triton X-100 and 0.05% Tween 20 in PBS for 30 min. They were then incubated overnight with primary antibodies (anti-GluN2B and anti-p-Y1472, 1:200) in blocking solution at 4 °C. After washing with PBS three times, fluorescent Alexa 488-conjugated secondary antibody was applied to the cells on coverslips at room temperature for 2 h, and the coverslips were then washed with PBS three times. The coverslips were then mounted on slides with antifade mounting medium containing DAPI (Beyotime Biotechnology, Shanghai, China). Images were acquired by laser scanning confocal microscopy (LSM710, Zeiss, Japan) and analyzed with ImageJ software. The area of interest was selected, the

**Table 1** Primary antibodies used in this study

| Antibody | Specificity | Type | Species | Source (catalog number) |
|---|---|---|---|---|
| Anti-GluN1 | GluN1 | pAb | Rabbit | ABclonal (A7677) |
| Anti-GluN2A | GluN2A | mAb | Rabbit | ABclonal (A19089) |
| Anti-GluN2B | GluN2B C-terminus | pAb | Rabbit | ABclonal (A3056) |
| Anti-p-Y1472 | p-GluN2B (Y1472) | pAb | Rabbit | Cell Signaling Technology (4208) |
| Anti-STEP | STEP (23E5) | pAb | Mouse | Cell Signaling Technology (4396) |
| Anti-np-S221 | np-STEP (S221) (D74H3) | mAb | Rabbit | Cell Signaling Technology (5659) |
| Anti-FYN | FYN | mAb | Mouse | ABclonal (A0086) |
| Anti-p-Y416 | p-Sar family Y416 | pAb | Rabbit | ABclonal (RK06002) |
| Anti-PP1CA | PP1CA (a.a 1–330) | pAb | Rabbit | ABclonal (A12468) |
| Anti-p-T320 | p-PP1CA T320 | pAb | Rabbit | ABclonal (AP0786) |
| Anti-DARPP-32 | DARPP-32 | pAb | Rabbit | Abmart (Q9UD71) |
| Anti-p-T34 | p-T34 DARPP-32 | pAb | Rabbit | Abcam Ab254063 |
| Anti-APP | APP (APP695, APP770, APP751) | pAb | Rabbit | Cell Signaling Technology (2452) |
| Anti-APPβ | sAPPβ | pAb | Rabbit | IBL (18,957) |
| Anti-BACE1 | BACE1 (D10E5) | mAb | Rabbit | Cell Signaling Technology (5606) |
| Anti-PS1 | PS1 | pAb | Rabbit | Cell Signaling Technology (3622) |
| Anti-AEP | Legumain (D6S4H) | mAb | Rabbit | Cell Signaling Technology (93,627) |
| Anti-IDE | IDE | pAb | Rabbit | Abcam (ab32216) |
| Anti-NEP | CD10/MME | pAb | Rabbit | ABclonal (A5664) |
| Anti-LRP1 | LRP1 | pAb | Rabbit | ABclonal (A13509) |
| Anti-PSD-95 | PSD-95 N-terminal | mAb | Rabbit | Cell Signaling (2507) |
| Anti-Synapsin1 | Synapsin1 | pAb | Rabbit | Millipore (AB1543) |
| Anti-GFAP | GFAP C-terminus | pAb | Rabbit | ABclonal (A14673) |
| Anti-IBA1 | AIF1/IBA1 | mAb | Rabbit | ABclonal (A19776) |
| Anti-β-actin | β-actin | pAb | Rabbit | ABclonal, China (AC026) |

*p*- phosphorylated, *np*- nonphosphorylated, *pAb* polyclonal antibody, *mAb* monoclonal antibody

threshold was adjusted, and then, the integrated density of the fluorescence in the area of interest was computed.

## PP2B Activity Assay

This assay is based on the detection of the free phosphate released based on the classic malachite green assay. Supernatants from primary neuron lysates and mouse brain tissue extracts were prepared with the provided lysis buffer. PP2B activity in the supernatants was assayed using the Cellular Calcineurin Phosphatase Activity Assay Kit (Colorimetric) (ab139464) according to the manufacturer's instructions (Abcam, Boston, MA, USA). Briefly, endogenous free phosphate was first removed from the supernatants. The background, total phosphatase activity, total phosphatase activity less PP2B, and the positive control wells were prepared in duplicate for each sample. Ten microliters of calcineurin substrate were added to each well of the calcineurin samples except for the "Background" control and equilibrated for 10 min at 30 °C. Then, 5 µL of extract or diluted calcineurin was added to the appropriate wells, which were then incubated for 30 min at 30 °C. The reactions were terminated by adding 100 µL of Green Assay Reagent, and the color was allowed to develop for 30 min. Phosphate release from the substrate was detected by measuring the absorbance of a molybdate-malachite green-phosphate complex at 620 nm. The PP2B activity equals total phosphatase activity minus total phosphatase activity less PP2B.

## Calcium Staining

The calcium indicator Fluo-8 AM (ab142773, Abcam, CA, USA) was used to measure the intracellular $Ca^{2+}$ changes in each group of primary culture neurons, and the procedures were performed as previously described with little modification [53]. Briefly, mouse primary hippocampal neurons were prepared and plated in 60-mm plastic culture dishes. The neurons were cultured for 14 days, and half of the maintenance medium was replaced every 3 days. Two milliliters of 4 µM Fluo-8 AM in artificial cerebrospinal fluid (aCSF, containing 124 mM NaCl, 25 mM $NaHCO_3$, 2.5 mM KCl, 1 mM $KH_2PO_4$, 2 mM $CaCl_2$, 2 mM $MgSO_4$, and 10 mM glucose) was added to the neuronal cells for 30 min at 37 °C and 5% $CO_2$ to load the dye into the hippocampal neurons. Then, the cells were washed three times and incubated for 1 h in aCSF with or without FA at 37 °C and 5% $CO_2$. The

cells were observed under a microscope, and target cells were selected. Then, the resting fluorescence was recorded in aCSF for 5 min, and 2 μM Aβ oligomers were added to stimulate $Ca^{2+}$ influx. Fluorescent signals in individual hippocampal neurons were recorded from the soma using laser scanning confocal microscopy (LSM710, Zeiss, Japan). The change in free intracellular calcium is proportional to the change in the fluorescence intensity of Fluo-8. The background intensity was subtracted from the measured intensity, and the fluorescence changes over time and the normalized average fluorescence intensity of Fluo-8 were calculated. The ratio of $\Delta F$ [stimulation intensity ($F_{stim}$) minus resting intensity ($F_{rest}$)] by $F_{rest}$ ($\Delta F/F$) corrected to the decay was computed. $\Delta F/F$ represents the relative changes in intracellular free $Ca^{2+}$ with a $\Delta F/F$ of 1 indicating a 100% increase in intracellular $Ca^{2+}$.

## Animals

Three-month-old male APP/PS1 mice (B6.Cg-Tg(APPswe, PSEN1dE9)85Dbo/Mmjax under C57BL/6 J) were purchased from Cavins Laboratory Animal Co., Ltd. (Changzhou), and wild-type (WT) C57BL/6 J mice were purchased from the Experimental Animal Centre of Tongji Medical College. The animals were housed with four to five littermates in ventilated cages in a thermoregulated and pathogen-free environment. The mice were kept under a 12-h/12-h light/dark cycle with free access to food and water. All animal protocols were performed according to the guidelines of the Huazhong University Animal Care and Use Committee.

## Ferulic Acid Treatment

Three-month-old male APP/PS1 and WT mice were divided into 3 groups: WT C57BL/6 J as a control, APP/PS1 as the AD model, and APP/PS1 with FA treatment as the treatment group. Mice were allowed to acclimatize to the laboratory environment for 2 weeks, during which time their water intake was evaluated. According to the measured body weight of the mice and the experimental conditions, the average amount of water drank by each mouse per day was estimated to be 4–5 mL. FA was purchased from MedChemExpress LLC (Shanghai, China) and solubilized in 10% DMSO, 40% PEG300, 5% Tween-80, and 45% saline to a stock concentration of 5 mg/mL and then resuspended in drinking water to a concentration of 50 mg/kg/day in 5 mL. It was thus estimated that the mice would have an average FA consumption of 50 mg/kg/day. With an average mouse weight of 20 g, every mouse was administered 1 mg of FA in 5 ml of drinking water that contained 0.04% DMSO, 0.16% PEG300, 0.02 Tween-80, and 0.18% saline. The vehicle control in AD (APP/PS1) and WT (C57BL/6 J) mice was normal drinking water with the same percentage of solvents but without FA. The bottles of water were changed every day, and the treatment lasted for 4 months.

## Behavioral Tests

The order in which the animals were subjected to each behavioral test was randomized between litters. All behavioral testing apparatuses were wiped down with 75% ethanol between animals and trials. All scoring was performed by researchers blinded to both the genotypes and the treatments. All testing was performed in a dimly lit room with mice at 7.5 to 8 months of age.

## Morris Water Maze (MWM) Test

To evaluate spatial learning, the mice were subjected to the MWM test. The apparatus (MWM, Techman Software Co., Ltd., Chengdu, China) consisted of a circular tank with a diameter of 1.2 m and a height of 50 cm, above which a camera was fixed. Visual cues of different shapes were placed around the water tank. The water was maintained at a temperature of $22 \pm 1$ °C and made opaque using milk powder. A 10-cm circular platform was placed 0.5 cm under the water surface at a fixed position in a target quadrant. Before the test began, the mice were habituated to the behavioral testing room, and the acquisition phase was conducted for 6 days, with each trial lasting 60 s and each animal being subjected to 3 trials per day. If a mouse could climb onto the platform within 60 s, it was allowed to stay on the platform for 20 s; otherwise, at the end of the 60 s, the mouse was guided to the platform and allowed to stay for 20 s. The latency time (s) to find the hidden platform was recorded after each trial of each learning session. Twenty-four hours after the end of the training, the hidden platform was removed, and the mice were placed into the pool for the probe trial. The duration of the probe trial was 60 s, and then, the latency to cross the platform location and the number of platform crossings, as well as the time in the target quadrant and the total distance covered, were all recorded.

## Open Field Test (OFT)

The OFT was applied to assess the anxiety and spontaneous movements of the mice. The apparatus (Techman Software Co., Ltd., Chengdu, China) was a plastic container consisting of an open field arena ($50 \times 50 \times 50$ cm), and a digital camera was positioned directly above the center of the field. The square field was divided into $5 \times 5$ zones, and the middle $3 \times 3$ sectors were defined as the center area. Each mouse was gently placed in the open field arena and allowed to freely explore for 5 min. The distance traveled and the center duration were both recorded by a camera system.

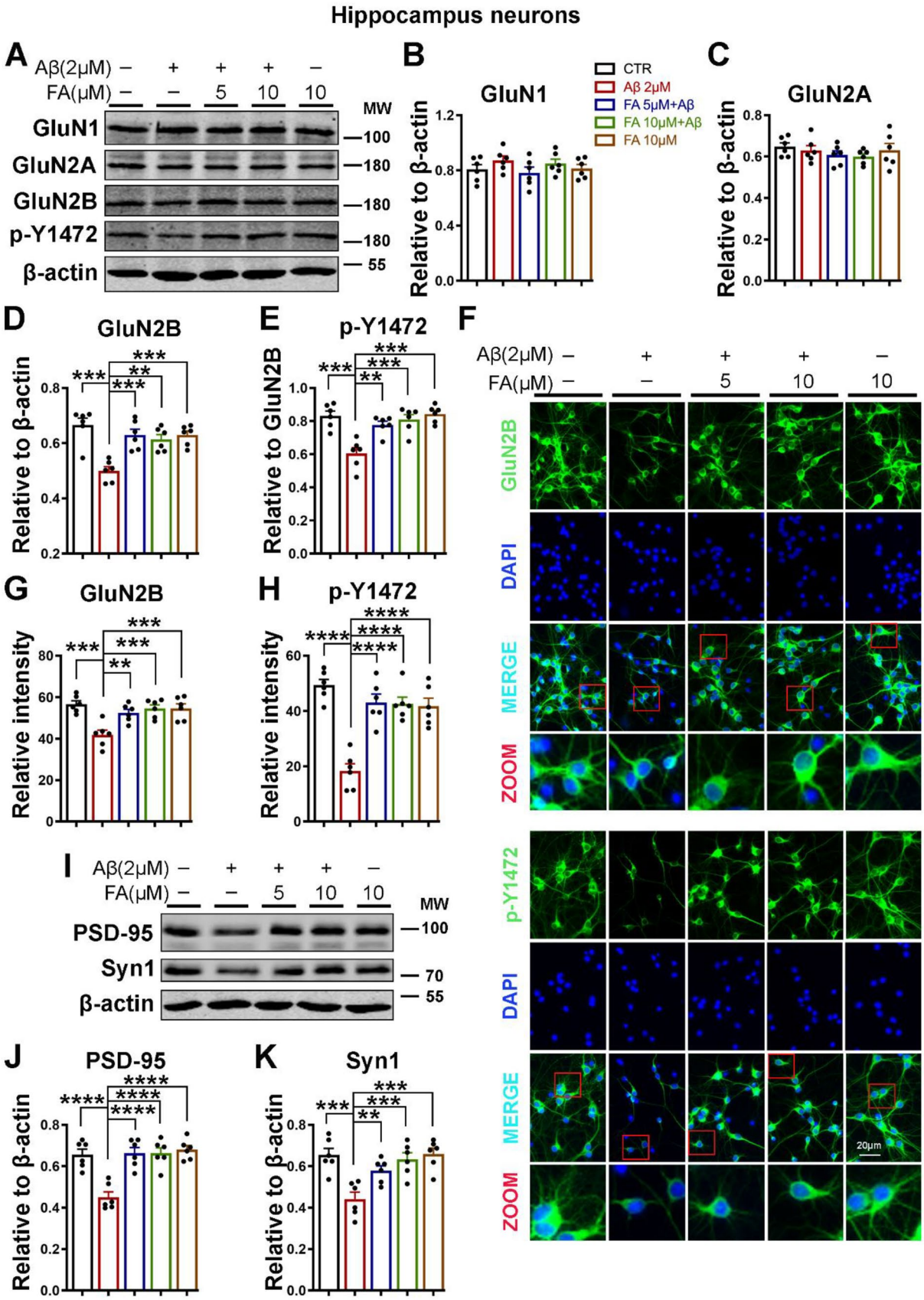
Hippocampus neurons
A
Aβ(2μM) – + + + –
FA(μM) – – 5 10 10
MW
GluN1
GluN2A
GluN2B
p-Y1472
β-actin
100
180
180
180
55
B
GluN1
CTR
Aβ 2μM
FA 5μM+Aβ
FA 10μM+Aβ
FA 10μM
Relative to β-actin
C
GluN2A
Relative to β-actin
D
GluN2B
Relative to β-actin
E
p-Y1472
Relative to GluN2B
F
Aβ(2μM) – + + + –
FA(μM) – – 5 10 10
GluN2B
DAPI
MERGE
ZOOM
p-Y1472
DAPI
MERGE
ZOOM
20μm
G
GluN2B
Relative intensity
H
p-Y1472
Relative intensity
I
Aβ(2μM) – + + + –
FA(μM) – – 5 10 10
MW
PSD-95
Syn1
β-actin
100
70
55
J
PSD-95
Relative to β-actin
K
Syn1
Relative to β-actin

◂**Fig. 1** FA preincubation prevents the Aβ-induced loss of synaptic proteins. **A** The expression of GluN1, GluN2A, GluN2B, and p-Y1472 was evaluated by western blotting in neuronal cell lysates treated with Aβ with or without 2 h of preincubation with FA. **B**–**E** Statistical analysis of western blot data from **A**. **F** Representative immunofluorescence images of neurons using GluN2B and p-Y1472 GluN2B antibodies following Aβ induction with or without 2 h of FA preincubation (scale bar = 20 μm). **G**, **H** Statistical analysis of immunofluorescence data from **F**. **I** The expression levels of PSD-95 and Synapsin1 were evaluated by western blotting with lysates of neuronal cells treated with Aβ with or without preincubation with FA. **J**, **K** Statistical analysis of western blot data from **I**. β-Actin served as the loading control. The results are from three independent experiments ($n = 6$), and the data are presented as the mean ± SEM. $^{**}p < 0.01$; $^{***}p < 0.001$; and $^{****}p < 0.0001$ vs. control or vs. Aβ treatment groups. p-Y1472, phosphorylated GluN2B at Tyr1472

## Novel Objective Recognition (NOR) Test

The mice were placed in an area (50 × 50 × 50 cm plastic container) for 5 min without any other object and allowed to rest for 24 h in the test room before the experiment was carried out. On the first day of testing, objects A and B (with different shapes and colors) were placed in two corners of the box, and the mice were placed in the area from the center and were allowed to explore objects A and B for 5 min. After 24 h, object B was replaced by object C (the shape and color of object C were different from those of objects A and B). The time the mice explored objects A, B, and C was recorded. The recognition index was calculated as TA / (TA + TC) and TC / (TA + TC) on the second day. TA and TC represent the time the mice explored objects A (old) and C (new), respectively.

## Fear Conditioning Tests

The experiment was performed in a white chamber (33 × 33 × 33 cm) equipped with a transparent front door, a grid floor, and a speaker. The mice were habituated to a training chamber for 3 min. On the first day, a tone (20 s, 80 dB, 2000 Hz), the conditioned stimulus (CS), was given and immediately followed by a short-term foot shock (2 s, 0.8 mA), the unconditioned stimulus (US). Each mouse received three CS-US pairings with a 60-s interval during the trial. Twenty-four hours (second day) after conditioning, the mice were re-exposed to the original training chamber for 5 min for the context-dependent test, during which no tones or shocks were presented. After another 24 h (third day), the cue-dependent test was carried out with different contextual cues. For this test, novel cardboard (plastic floor) was placed on the top of the grid floor to provide a different tactile sensation, and vinegar drops and yellow walls were used to change the color and odor. Each mouse was placed in the original context for 5 min in total without a shock. After 2 min of free exploration, the mouse was exposed to the same 3 CS tones with a 20-s intertrial interval. The freezing responses in both the context and cued conditions were recorded.

## Electrophysiology

The mice were deeply anesthetized and sacrificed, and their brains were quickly collected. The brains were frozen in ice-cold oxygenated (95% $O_2$, 5% $CO_2$) artificial cerebrospinal fluid (aCSF, containing mM 124 NaCl, 2.5 KCl, 2 $CaCl_2$, 2 $MgSO_4$, 1 $NaH_2PO_4$, 25 $NaHCO_3$, and 10 glucose; pH 7.4) and horizontally sliced at a thickness of 300 μm with a vibratome (Leica, Germany). The slices were allowed to recover in aCSF at 29 °C for 90 min. A single slice was transferred to an MED probe (MED-P515A, 8 × 8 array, interpolar distance 150 μm, Panasonic) and perfused with 29 °C aCSF at a flow rate of 2 mL/min. The electrodes were placed in the dentate gyrus (DG, stimulated region) and CA3 region (recording region). Field excitatory postsynaptic potentials (fEPSPs) were recorded at DG-CA3 synapses. Electrical stimulation was delivered to one channel within the DG, and evoked fEPSPs were recorded from the other 63 channels. The stimulation intensity was approximately 40% of the intensity required to induce maximal fEPSPs. To record LTP, baseline responses were evoked for at least 30 min until stabilization, and then, a high-frequency stimulation (HFS), consisting of 10 bursts, each containing 4 pulses at 100 Hz with an interburst interval of 200 ms, was applied at a stimulation intensity that was adjusted to elicit 40% of the maximal response. After the application of the HFS protocol, the test stimulus was repeatedly delivered once every minute for 1 h to record LTP [54, 55].

## Thioflavin S Staining

The mice were deeply anesthetized and then intracardially perfused with saline and 4% paraformaldehyde. The brains were collected, postfixed for 24 h in 4% paraformaldehyde, and dehydrated in 30% sucrose solution until they sank to the bottom before being coronally sectioned with a cryotome (CM1950, Leica, Nussloch, Germany) at a thickness of 25 μm, and the free-floating sections were preserved in antifreeze solution (40% PBS, 30% glycerol, 30% ethylene glycol) at − 20 °C until use. Thioflavin S staining (Ths) was used to label the Aβ plaques. Briefly, 25-μm cryotome-sectioned brain slices were washed three times in PBS and then stained with ThS (T1892-25G, Sigma-Aldrich, Shanghai, China) (12.5 mg/mL) in 50% ethanol in the dark for 5–10 min at room temperature, followed by two washes with 50% ethanol and PBS and another 2 washes in PBS. Finally, the slides were sealed using 50% glycerin in PBS. Images of the whole brain section were obtained using an Olympus VS120 slide scanner system (Tokyo, Japan). The regions of

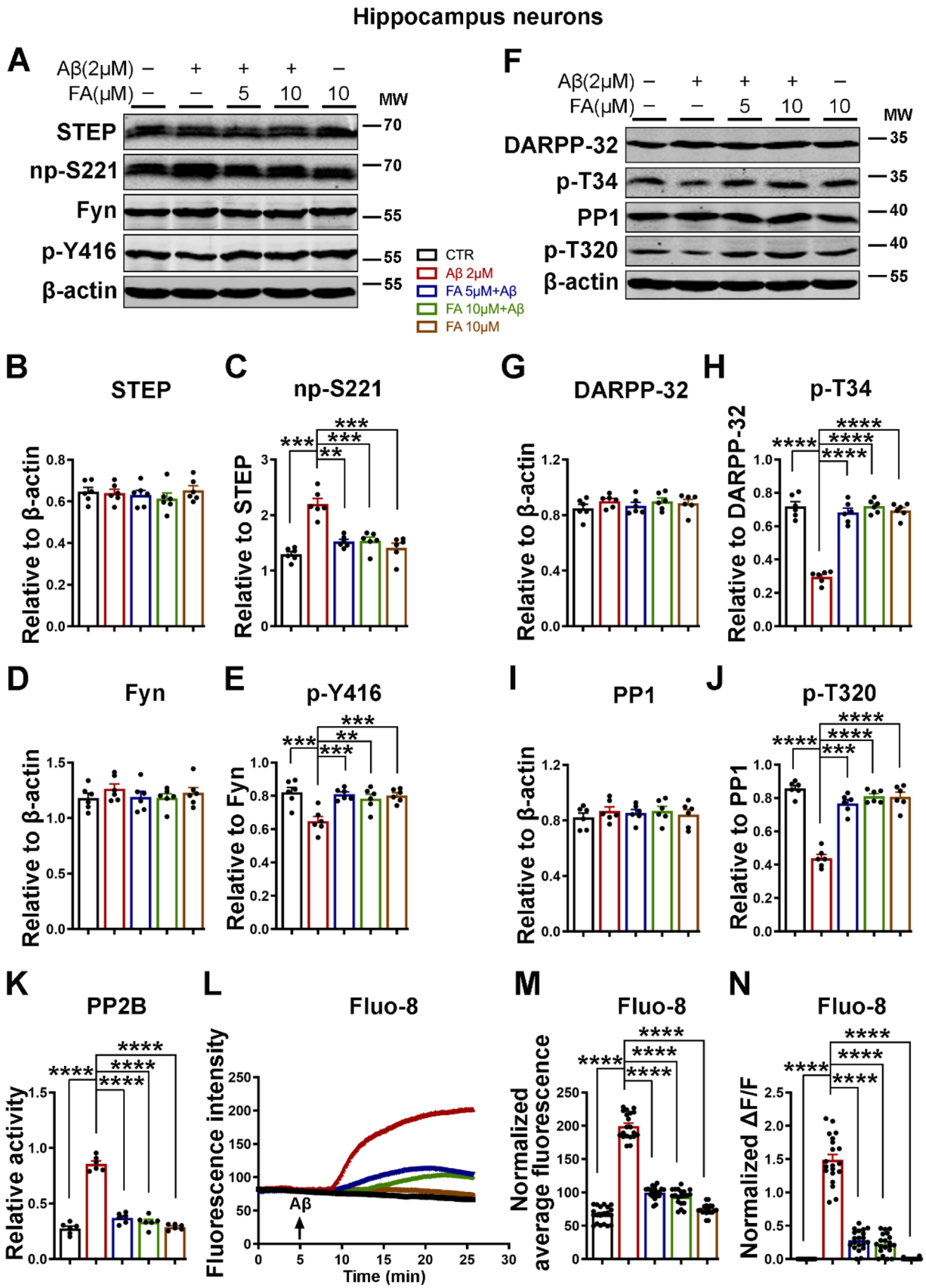
Hippocampus neurons
A
Aβ(2μM) – + + + –
FA(μM) – – 5 10 10
MW
STEP
np-S221
Fyn
p-Y416
β-actin
70
70
55
55
55
CTR
Aβ 2μM
FA 5μM+Aβ
FA 10μM+Aβ
FA 10μM
F
Aβ(2μM) – + + + –
FA(μM) – – 5 10 10
MW
DARPP-32
p-T34
PP1
p-T320
β-actin
35
35
40
40
55
B
STEP
Relative to β-actin
C
np-S221
Relative to STEP
G
DARPP-32
Relative to β-actin
H
p-T34
Relative to DARPP-32
D
Fyn
Relative to β-actin
E
p-Y416
Relative to Fyn
I
PP1
Relative to β-actin
J
p-T320
Relative to PP1
K
PP2B
Relative activity
L
Fluo-8
Fluorescence intensity
Aβ
Time (min)
M
Fluo-8
Normalized average fluorescence
N
Fluo-8
Normalized ΔF/F

◂**Fig. 2** FA prevents the Aβ-induced STEP-mediated decrease in p-Y1472 GluN2B via the calcium-related PP2B/DARPP-32/PP1 axis. **A** The expression levels of STEP, Fyn, np-S221, and p-Y416 were evaluated by western blotting in neuronal cell lysates treated with Aβ with or without 2 h of preincubation with FA. **B**–**E** Statistical analysis of western blot data from **A**. **F** The expression levels of DARPP-32, PP1, p-T34, and p-T320 were evaluated by western blotting in neuronal cell lysates treated with Aβ with or without 2 h of preincubation with FA. **G**–**J** Statistical analysis of western blot data from **F**. β-Actin served as the loading control ($n=6$). **K** PP2B (calcineurin) activity was measured using the PP2B activity kit ($n=6$). **L–N** Calcium staining experiments ($n=20$). **L** Fluorescence intensity and **M** normalized average fluorescence intensity of Fluo-8 indicate intracellular calcium level changes in the neuronal cells. **N** The ratio of $\Delta F$ [stimulation intensity ($F_{stim}$) – resting intensity ($F_{rest}$)] to $F_{rest}$ ($\Delta F/F$) is the change in fluorescence intensity relative to the resting fluorescence intensity. The results are from three independent experiments, and the data are presented as the mean ± SEM. $^{**}p<0.01$; $^{***}p<0.001$; and $^{****}p<0.0001$ vs. control or vs. Aβ treatment groups. np-S221, nonphosphorylated STEP at Ser221; p-Y416, phosphorylated Fyn at Tyr416; p-T34, phosphorylated DARPP-32 at Thr34; p-T320, phosphorylated PP1 at Thr320

interest (cortex and hippocampus) were selected and analyzed using ImageJ software while adjusting the threshold to differentiate the Aβ plaque fluorescence from the background, and then, the area% of the fluorescence in the region of interest was computed.

### ELISA for Aβ40/42, IL-1β, and TNF-α

The mouse hippocampi were homogenized in PBS (containing 1:100 PMSF and 1:100 protease inhibitor cocktail), and the homogenate was centrifuged for 10 min at 12,000 g at 4 °C. The supernatant was collected as the RIPA-soluble fraction for the measurement of Aβ40/42, IL-1β, and TNF-α levels. The protein concentration in the supernatant was measured by the BCA method, and 200 μg of total protein in 100 μl PBS was added for the assay. The amounts of Aβ40 and Aβ42 were measured in soluble protein fractions by using a sandwich ELISA kit according to the manufacturer's instructions (Elabscience Biotechnology, Wuhan, China). The amounts of IL-1β and TNF-α were measured in soluble protein fractions by using a sandwich ELISA kit according to the manufacturer's instructions (ABclonal, Wuhan, China).

### Nissl Staining

Briefly, 25 μm cryotome-sectioned brain slices were washed three times in PBS and then mounted on gelatin-coated slides, and Nissl staining was performed according to the manufacturer's procedure (Beyotime Biotechnology, Shanghai, China). Slides were incubated in cresyl violet for 10 min at 25 °C; dehydrated through 50%, 75%, 95%, and 100% alcohol; cleared in xylene; and cover-slipped with neutral balsam. Pictures were taken using a light microscope (Nikon, Tokyo, Japan), the Nissl-stained neurons in the hippocampal CA3 regions were counted, and the thickness of the cortex was also measured by using ImageJ software.

### Golgi Staining

The mice were deeply anesthetized and intracardially perfused with normal saline. Their brains were collected and placed directly in Golgi solution (1 g potassium dichromate, 1 g mercuric chloride, 0.8 g potassium chromate, and 100 mL double-distilled water), where they remained in the dark for 2 weeks, with solution changes every 2 days. Thereafter, the brains were sequentially incubated in 10%, 20%, and 30% sucrose in light-protected jars to aid in maintaining the histological structure. The brains were then sectioned at 100-μm thickness with a vibratome (Leica, VT1000S, Nussloch, Germany) and placed on gelatin-coated glass slides. After rinsing with double-distilled water, the slides were incubated in ammonium hydroxide for 30 min. After being washed with water, the slides were incubated for 30 min in black and white film developer diluted 1:9 with water and then rinsed with double-distilled water. The brain slices were dehydrated in a gradient concentration of alcohol and transferred to a CXA solution containing formyl trichloride, xylene, and absolute ethyl alcohol (1:1:1) for 15 min. The slides were then cover-slipped and visualized under the microscope (Nikon, Tokyo, Japan), and intact dendritic branches in the hippocampal DG area were selected for spine counting. All subsequent quantitative analyses were conducted by researchers blinded to the groups.

### Statistical Analysis

All data are presented as the mean ± SEM and were analyzed using GraphPad Prism9 (GraphPad Software Inc., San Diego, CA, USA). Between-group differences were assessed by one-way analysis of variance followed by Tukey's post hoc test for multiple comparisons. Statistical significance was set at a 95% confidence interval, $p \leq 0.05$.

## Results

1. *Ferulic Acid Rescued the Aβ-Induced Decrease in NMDA Receptors and Other Synaptic Proteins*

Amyloid-β oligomers are believed to impair neuronal function and cognition, even before the appearance of overt toxicity [56]. One mechanism by which these soluble Aβ oligomers impair neuronal function is by promoting disturbances in glutamatergic neurotransmission [57], thus impairing synaptic function, which is essential for cognition. On the one hand, FA was found to improve learning and memory deficits, while on the other hand, synaptic

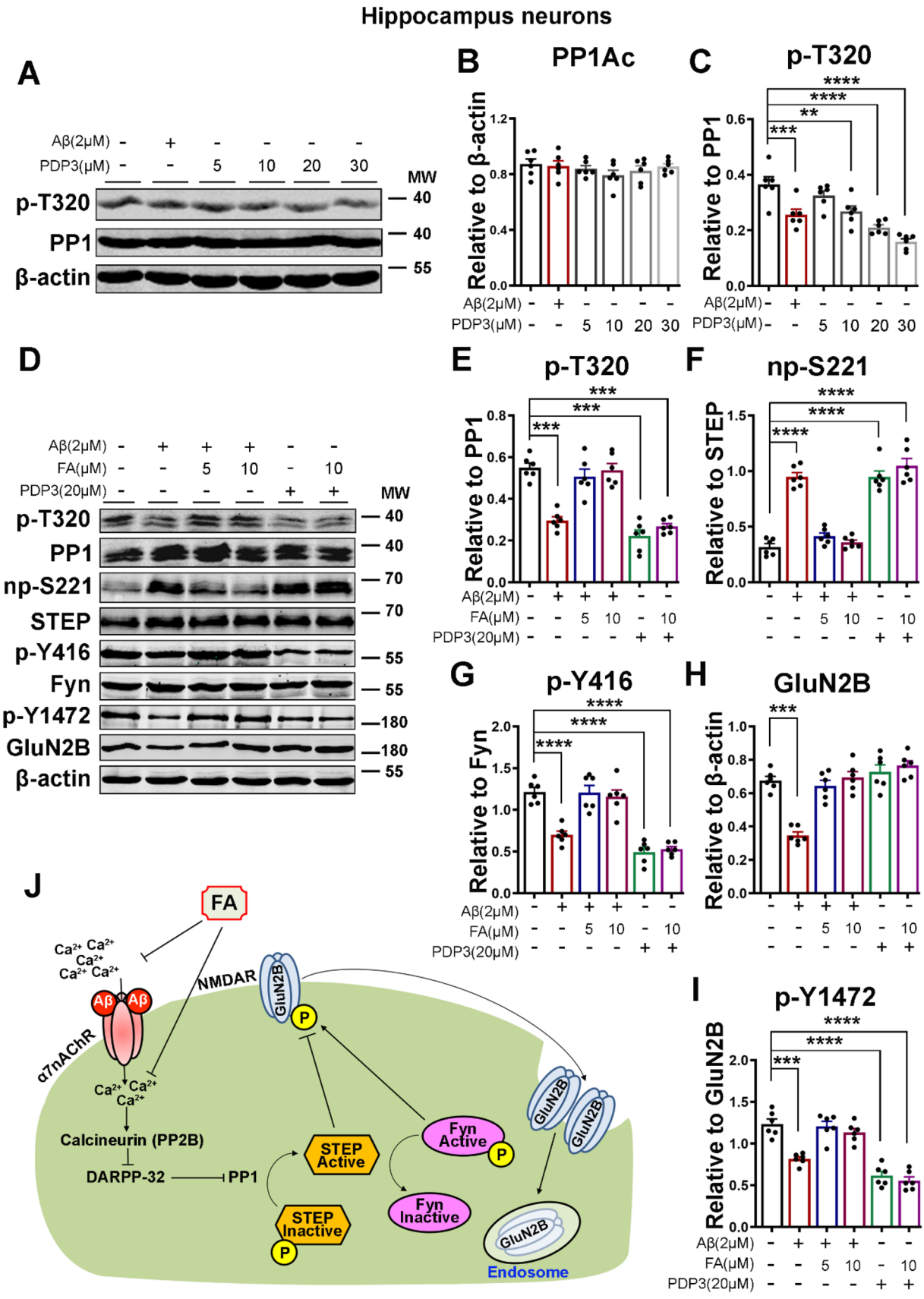
Hippocampus neurons
A
Aβ(2μM)
PDP3(μM)
MW
p-T320
PP1
β-actin
40
40
55
B
PP1Ac
Relative to β-actin
C
p-T320
Relative to PP1
D
Aβ(2μM)
FA(μM)
PDP3(20μM)
p-T320
PP1
np-S221
STEP
p-Y416
Fyn
p-Y1472
GluN2B
β-actin
70
70
55
180
180
E
p-T320
F
np-S221
Relative to STEP
G
p-Y416
Relative to Fyn
H
GluN2B
I
p-Y1472
Relative to GluN2B
J
FA
NMDAR
α7nAChR
Aβ
Ca2+
Calcineurin (PP2B)
DARPP-32
PP1
STEP Active
STEP Inactive
Fyn Active
Fyn Inactive
GluN2B
P
Endosome

◂**Fig. 3** FA acts upstream of PP1, as it does not recover the effect of direct activation of PP1 by PDP3. **A** The expression levels of PP1 and p-T320 in neuronal cells treated with Aβ or increasing concentrations of PDP3 were evaluated by western blotting. **B**, **C** Statistical analysis of PP1 and p-T320. **D** Representative western blot bands of the expression levels of PP1, p-T320, STEP, np-S221, Fyn, p-Y416, GluN2B, and p-Y1472 from lysates of primary neurons treated with Aβ or PDP3 with or without 2 h of FA preincubation. **E–I** Statistical analysis of data from **D**. No significant difference is found in the PP1, STEP, and Fyn levels. β-Actin served as the loading control ($n=6$). **J** Summary of the PP2B/DARPP-32/PP1 axis leading to the activation of STEP and a decrease in GluN2B phosphorylation. The results are from three independent experiments, and the data are presented as the mean ± SEM. $^{**}p<0.01$; $^{***}p<0.001$; and $^{****}p<0.0001$ vs. control group. p-T34, phosphorylated DARPP-32 at Thr34; p-T320, phosphorylated PP1 at Thr320; np-S221, nonphosphorylated STEP at Ser221; p-Y416, phosphorylated Fyn at Tyr416; p-Y1472, phosphorylated GluN2B at Tyr1472

impairments are observed in neurodegenerative diseases, including AD. To examine the effect of FA and Aβ on synaptic function, we harvested primary hippocampal neurons from mice, treated them with 2 μM Aβ oligomers with or without 2 h of pretreatment with FA, and evaluated different subunits of NMDARs. The western blot results showed that following Aβ treatment, the immunoreactivity of total and Tyr1472-phosphorylated GluN2B (p-Y1472 GluN2B) was significantly reduced, but the levels of GluN1 and GluN2A were not significantly different among the groups (Fig. 1A–E). To further confirm our results, we also carried out immunofluorescence experiments (Fig. 1F–H), and we found that the fluorescence intensity of total and p-Y1472 GluN2B-positive neurons was decreased following Aβ treatment. Interestingly, this decrease in the immunoreactivity of both total and p-Y1472 GluN2B, in both western blot and immunofluorescence experiments, was rescued when the neurons were pretreated with FA before Aβ incubation.

Synaptic architecture and integrity are important for normal synaptic function and thus for synaptic plasticity and learning and memory. Therefore, we also investigated changes in some synaptic proteins, including the presynaptic protein synapsin1 and postsynaptic density protein 95 (PSD-95). The results from our experiment revealed that the protein levels of synapsin1 and PSD-95 were significantly decreased by Aβ treatment, whereas treatment with FA before Aβ treatment helped prevent these changes in primary neuron cultures (Fig. 1I–K). Together, these data showed that Aβ is a stressor that triggers synaptic alterations in neurons that are prevented by preincubation with FA, indicating that FA might prevent the deleterious synaptic alterations induced by Aβ.

2. *Ferulic Acid Improved NMDA Receptor Alterations by Decreasing Aβ-Induced STEP Upregulation Through the PP2B/DARPP-32/PP1 Axis*

The phosphorylation of GluN2B and its surface expression are critical mechanisms for its functions and are mainly regulated by the protein tyrosine kinase Fyn [11, 58, 59] and the tyrosine phosphatase STEP [5, 11], which phosphorylate and dephosphorylate GluN2B at Tyr1472, respectively. To clarify how Aβ leads to the decreased phosphorylation of GluN2B, we evaluated the levels of Fyn and STEP by western blotting. Our results indicate that the total levels of both Fyn and STEP were not altered. Nevertheless, phosphorylated Fyn at Tyr416 (p-Y416, active form) was significantly decreased, whereas nonphosphorylated STEP at Ser221 (np-S221, active form) was significantly increased following Aβ treatment, and the treatment of primary neurons with FA before Aβ incubation prevented these changes (Fig. 2A–E).

The phosphorylation of STEP is mainly regulated by two main enzymes, cAMP-dependent protein kinase A (PKA) and PP1, which phosphorylate and dephosphorylate STEP, respectively [60, 61]. The activation of STEP could also be indirectly regulated by PP2B, which in the presence of increased intracellular calcium dephosphorylates (inactivates) DARPP-32, thereby removing the DARPP-32 inhibitory effect on PP1 [25, 61, 62]. Therefore, to understand how Aβ alters STEP phosphorylation, which was rescued by FA, we examined the PP2B/DARPP-32/PP1 axis. Interestingly, we found that both the phosphorylation of DARPP-32 at Thr34 (p-T34, active form) and the phosphorylation of PP1 at Thr320 (p-T320, inactive form) were significantly reduced following Aβ treatment, and again pretreatment with FA rescued this to a level comparable with that of the control (Fig. 2F–J).

To completely elucidate our theory, we measured PP2B activity, and the results revealed that Aβ induced a significant increase in PP2B activity, which was attenuated by FA preincubation (Fig. 2K). Furthermore, we used the calcium dye Fluo-8 and measured intracellular calcium changes in response to the Aβ stimulation of neurons in the presence of extracellular calcium with or without FA preincubation. Interestingly, the results showed that Aβ triggered a tremendous increase in intracellular calcium influx that was significantly attenuated by FA pretreatment (Fig. 2L–N). These results together indicate that Aβ triggers intracellular calcium influx to activate the PP2B/DARPP32/PP1 axis, which then results in STEP activation, and FA might act by attenuating Aβ-induced intracellular calcium influx to decrease STEP activity.

To demonstrate that the PP2B/DARPP-32/PP1 axis is at least one way by which Aβ induces an increase in STEP activity and that FA probably acts by decreasing intracellular calcium to decrease STEP activity, we used the PP1 activator PP1-disrupting peptide 3 (PDP3) to mimic the effect of Aβ. We first carried out an evaluation study to choose the appropriate concentration of PDP3. Primary neurons were incubated with Aβ and different concentrations of PDP3

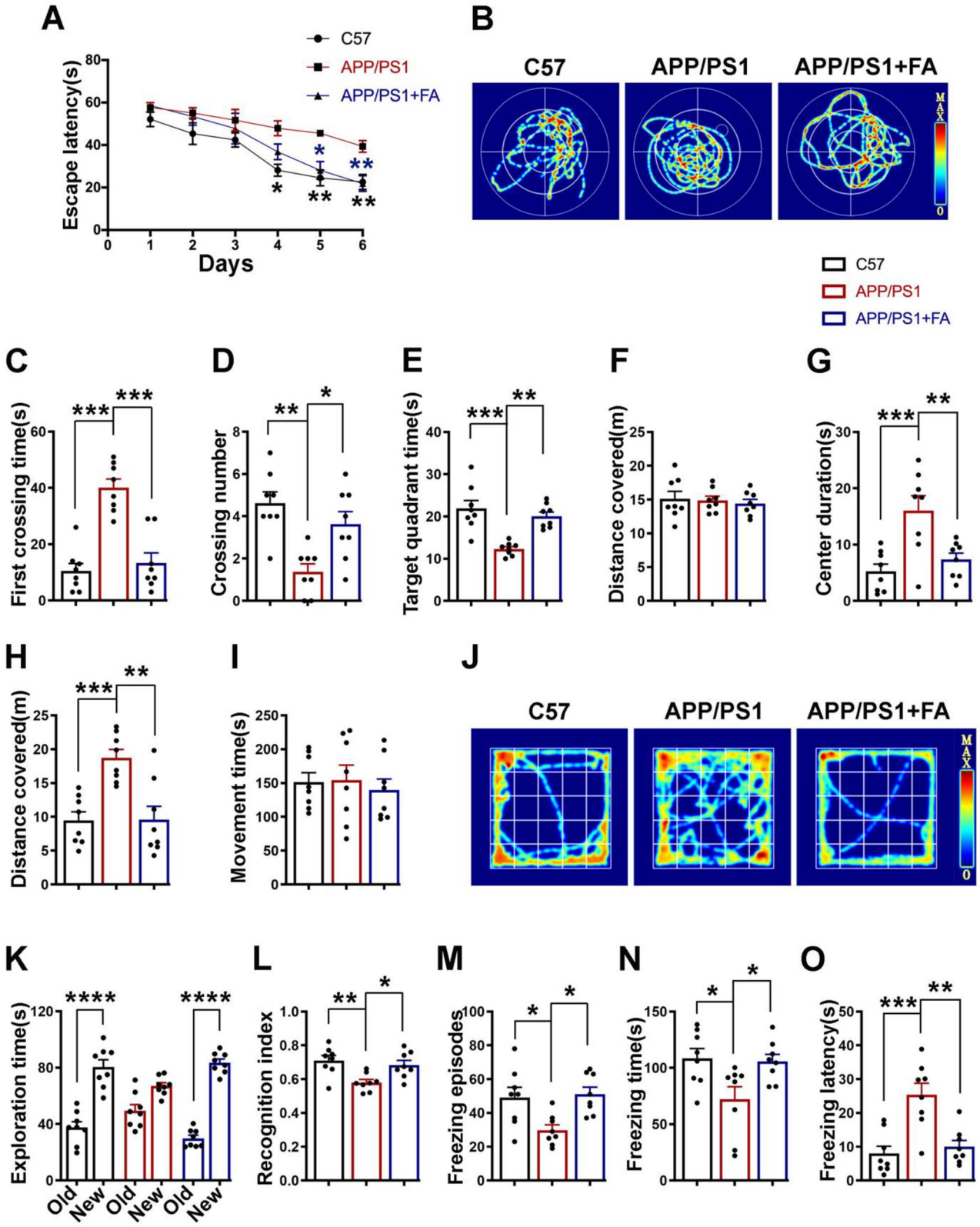


(Fig. 3A–C). On the basis of our experiment (Fig. 3A, C) and previous studies [63], a 20 μM concentration of PDP3 is enough to significantly activate PP1. We incubated neurons with Aβ or PDP3 with or without 2 h of FA preincubation, and the protein levels of total and np-S221 STEP, total and p-Y416 Fyn, and total and p-Y1472 GluN2B were evaluated

◂**Fig. 4** Long-term FA treatment prevents behavioral and cognitive deficits in APP/PS1 mice. **A**–**F** Morris water maze results. **A** Escape latency (s) of mice to find the platform during the six training days. **B** Representative searching traces of mice during the probe test. **C** The first crossing time (s), **D** The crossing number, **E** the time (s) spent in the target quadrant, and **F**. the total distance (m) covered by the mice during the probe test. **G**–**J** Open field test results. **G** Center duration (s). **H** distance (m) covered, **I**. movement time (s), and **J**. representative movement traces of mice during the 5 min of the test. **K, L** Novel object recognition test results. **K** The time (s) the mice explored the old and new objects during the test. **L** The recognition index. **M**–**O** Fear conditioning test results. **M** The number of freezing episodes. **N** The freezing time (s). **O** The freezing latency (s) during the test time. All behavioral tests were carried out from 7.5 to 8 months of age ($n=8$). Data are presented as the mean ± SEM. *$p<0.05$; **$p<0.01$; ***$p<0.001$; and ****$p<0.0001$ vs. control or vs. APP/PS1 mice groups

(Fig. 3D–I). Interestingly, when compared with the control, we found that, similar to Aβ treatment, PDP3 treatment induced an increase in the activity of PP1, as suggested by the decreased p-T320 PP1 (Fig. 3D, E). Subsequently, this results in an increased level of np-S221 STEP with a consequent decrease in p-Y416 Fyn and p-Y2472 GluN2B (Fig. 3D, F–I). Surprisingly, while FA pretreatment rescued Aβ-induced PP1 activation and its downstream effects (Figs. 1, 2, and 3), it did not affect PDP3-induced PP1 activation and its downstream effects (Fig. 3D–I), suggesting that the effect of Aβ that was abrogated by FA must be upstream of PP1, which might be due to increased intracellular calcium (Fig. 2L–N). These results together further indicate that Aβ induces STEP activation via the PP2B/DARPP-32/PP1 axis and that FA abrogates these effects, probably by decreasing intracellular calcium (Fig. 3J).

3. *APP/PS1 Mice Exhibited Behavioral and Cognitive Alterations that Were Prevented by Long-Term Administration of Ferulic Acid*

We have shown that Aβ induces alterations in synaptic integrity, including a decrease in total and p-Y1472 GluN2B as well as a decrease in PSD-95 and synapsin1, which together are critical players in synaptic plasticity. These alterations were significantly abrogated by FA preincubation before Aβ treatment in neurons. To further investigate the effects of Aβ on this calcium-related pathway and to determine whether FA would still have the same effect in an in vivo setting, we carried out animal experiments using Aβ AD model APP/PS1 mice. Three-month-old APP/PS1 mice were administered a 50 mg/kg/day dose of FA for 4 months, after which we carried out a panel of behavioral experiments, and we found that APP/PS1 mice exhibited memory and behavioral impairments that were absent in the C57 normal control mice as well as the FA-treated APP/PS1 mice (Fig. 4).

We first performed the Morris water maze test, and the results revealed that compared to the control mice, the APP/PS1 mice exhibited increased escape latency during the 6 days of training, whereas in the APP/PS1 mice supplemented with FA, the escape latency remained similar to that of the control mice (Fig. 4A). During the test, a longer latency period to cross the platform location, fewer platform location crossings, and less time spent in the target quadrant were observed in the APP/PS1 mice than in the control and FA-supplemented APP/PS1 mice (Fig. 4B–E). However, the distance covered remained unchanged among all three groups (Fig. 4F), suggesting normal motor function in these animals. Next, we performed an open field test, and the results revealed increases in the time spent in the center and the distance traveled by the APP/PS1 mice, which were absent in the C57 control mice as well as the FA-supplemented APP/PS1 mice, but the time spent moving was similar in all groups (Fig. 4G–J). This is an indication of anxiety and restlessness in the APP/PS1 mice. We also carried out a novel object recognition test, the results of which revealed increased time spent exploring the new object, as well as a higher recognition index, in both the C57 control mice and the APP/PS1 mice supplemented with FA when compared with the APP/PS1 mice (Fig. 4K, L). Finally, we performed a fear conditioning test. The contextual fear memory test results showed fewer freezing episodes, a lower freezing time, and an increased freezing latency in the APP/PS1 mice than in the C57 control mice and APP/PS1 mice supplemented with FA (Fig. 4M–O). The cued fear memory results (data not shown) were not different among the groups. Together, these results are a clear indication of learning, memory, and behavioral deficits in the APP/PS1 mice, all of which were significantly abrogated by FA supplementation in these animals, suggesting a protective effect of FA against synaptic impairments.

4. *APP/PS1 Mice Exhibited Increased Aβ Protein Levels and More Plaques, Both of Which Were Prevented by Long-Term Ferulic Acid Aupplementation*

APP/PS1 mice are an Aβ model of AD that exhibit behavioral, learning, and memory deficits as a result of increased Aβ accumulation as age progresses. In these mice, amyloid plaques begin to be deposited at the age of 6 weeks in the cortex and at approximately 3–4 months in the hippocampus, while cognitive dysfunctions are reported at the age of 6–7 months [64–66]. Moreover, Aβ is established to be the trigger in AD pathogenesis [67–72], and Aβ toxicity is known to induce synaptic dysfunction [73]. In light of these previous reports and our primary neuron results, we speculated that FA might reduce the Aβ burden in treated animals. We first carried out a western blot experiment on hippocampal brain lysates, and as expected, APP/PS1 mice exhibited an increase in the total APP protein level compared to the C57 control mice, and

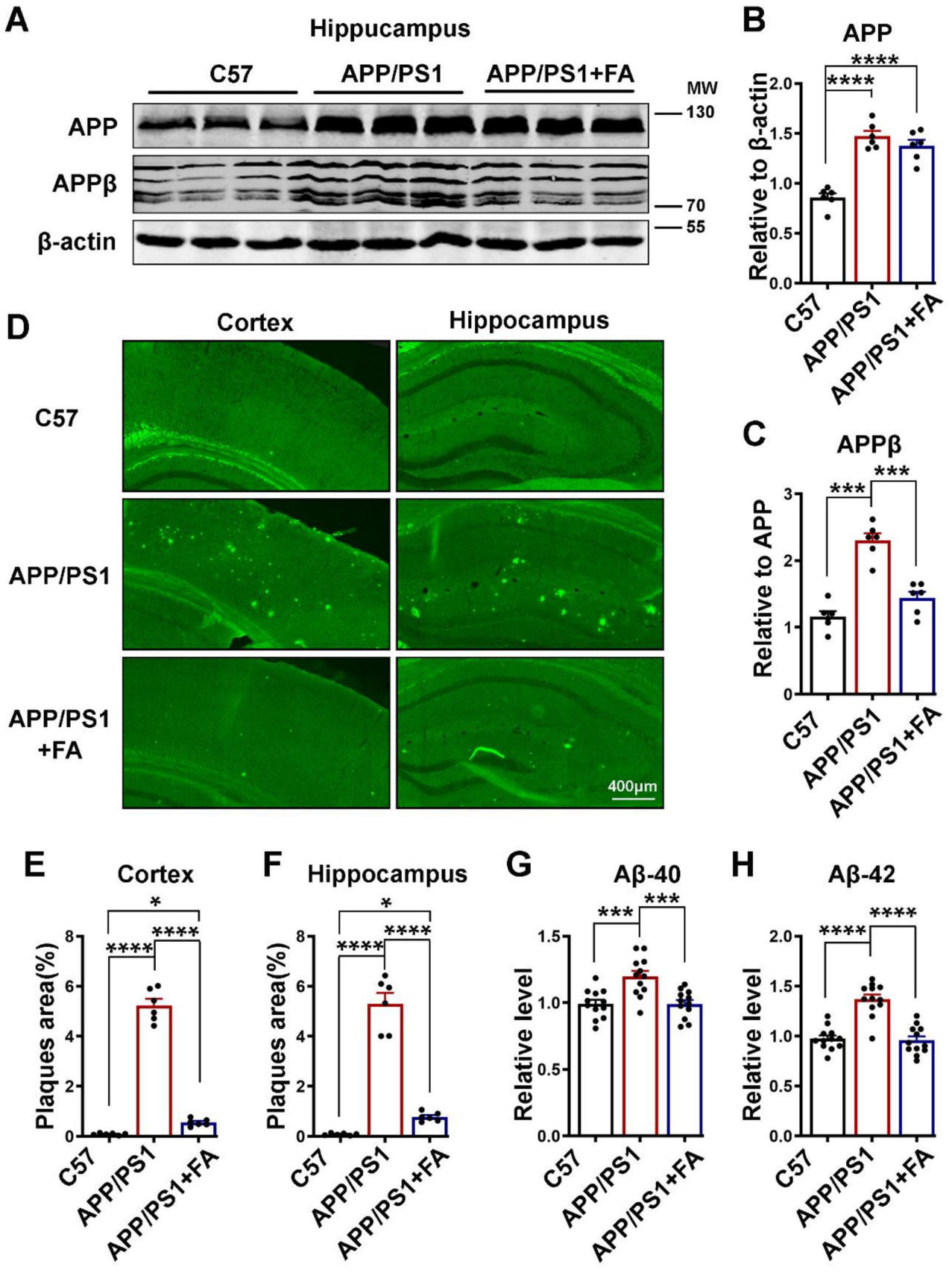
A
Hippucampus
C57
APP/PS1
APP/PS1+FA
MW
130
70
55
APP
APPβ
β-actin
B
APP
Relative to β-actin
C57
APP/PS1
APP/PS1+FA
C
APPβ
Relative to APP
D
Cortex
Hippocampus
C57
APP/PS1
APP/PS1 +FA
400μm
E
Cortex
Plaques area(%)
F
Hippocampus
G
Aβ-40
Relative level
H
Aβ-42

◂**Fig. 5** Long-term FA treatment alleviates the Aβ burden in APP/PS1 mice. **A** The expression of APP and APPβ in hippocampal lysates of C57 control and APP/PS1 mice with or without long-term FA treatment was evaluated by western blotting. β-Actin served as the loading control ($n=6$). **B**, **C** Statistical analysis of APP and APPβ. **D** Representative images of thioflavin S staining from C57 control and APP/PS1 mice with or without long-term FA treatment (scale bar = 400 μm, $n=6$, from 3 mice and 2 images were analyzed per mouse). **E**, **F** The quantification of thioflavin S fluorescence shows the % of Aβ plaque area pixels divided by the full area captured in the cortex and hippocampus. **G**, **H** Statistical analysis of the ELISA results for Aβ40 and Aβ42 from hippocampal lysates of C57 control and APP/PS1 mice with or without long-term FA treatment. $N=12$; 6 mice per group and 3 independent experiments. The data are presented as the mean ± SEM. $*p<0.05$; $***p<0.001$; and $****p<0.0001$ vs. control or vs. APP/PS1 mice groups

FA treatment had no effect on the APP level (Fig. 5A, B). We then evaluated the APPβ level, and interestingly, when compared with the APP/PS1 mice drinking normal water, the FA-supplemented group of APP/PS1 mice showed a significantly lower level of this toxic protein, and this level was comparable to that in the C57 control mice (Fig. 5A, C). Next, we performed thioflavin S staining, and we found results that were similar to those of western blotting. Significantly more plaques were observed in both the cortex and the hippocampus of the APP/PS1 mice than in the C57 control and the FA-supplemented APP/PS1 mice (Fig. 5D–F). To further confirm our results, we performed Aβ ELISA on brain hippocampal lysates. Both Aβ40 (Fig. 5G) and Aβ42 (Fig. 5H) were found to be significantly lower in the FA-supplemented group than in the group without supplementation, and this level was comparable to that in C57 control mice. These results together indicate that the Aβ buildup that is characteristic of APP/PS1 mice is significantly reduced by FA supplementation and that this might be at least in part responsible for the improved behavioral and cognition functions observed in the APP/PS1 mice with FA supplementation.

5. *The Reduced Aβ Load in Ferulic Acid-Supplemented APP/PS1 Mice Was the Result of the Modulation of Both Production and Clearance Pathways*

The increased Aβ accumulation in AD is the result of increased APP cleavage by BACE1 and γ-secretase [17, 18] as well as an age-associated decrease in Aβ clearance [74–77]. To investigate how FA reduces Aβ load in APP/PS1 mice, we evaluated both the production and clearance of Aβ. We found that FA supplementation reduced BACE1, the rate-limiting enzyme in Aβ production, to a level comparable with that of the C57 control mice, while the level of PS1, the catalytic subunit of γ-secretase, remained unchanged (Fig. 6A–C). Asparagine endopeptidase (AEP), a pH-controlled cysteine proteinase, is reported to cleave APP at N585, BACE1 at N294, and Tau at N368 to mediate AD [78–83]. Thus, we evaluated the AEP level in APP/PS1 following FA supplementation. We found that the protein level of mature AEP was higher in APP/PS1 mice than in C57 control mice, and interestingly, FA supplementation significantly reduced the AEP level compared to that in APP/PS1 mice without FA supplementation, even though this level was still higher than that in C57 control mice (Fig. 6A, D). The protein levels of clearance-associated proteins, including insulin-degrading enzyme (IDE), neprilysin (NEP), and low-density lipoprotein receptor-related protein 1 (LRP1), were found to be decreased in APP/PS1 mice compared to C57 control mice, and FA supplementation in these mice was associated with a significant increase in these proteins compared to mice without FA supplementation (Fig. 6A, E–G).

6. *APP/PS1 Mice Exhibited a Decrease in p-Y1472 GluN2B and an Increase in STEP, Which Were Both Abrogated by Ferulic Acid Supplementation*

We have shown in neuronal cell culture that FA preincubation was able to prevent Aβ-induced synaptic impairments, and it is known that synaptic dysfunction is a characteristic of AD that translates to the behavioral and cognitive deficits observed in different stages of AD [19]. Thus, we evaluated the expression of NMDA receptors, which are critical players in synaptic plasticity and therefore cognition. The protein levels of GluN1, GluN2A, GluN2B, and p-Y1472 GluN2B were evaluated by western blotting (Fig. 7A–E). Consistent with the neuronal cell experiments, the levels of GluN1 and GluN2A were not different (Fig. 7A–C); however, in contrast to the cell experiments where Aβ induced a decrease in both total and p-Y1472 GluN2B, only p-Y1472 GluN2B was found to be significantly decreased in the APP/PS1 mice compared to the C57 control mice and the APP/PS1 mice with FA supplementation (Fig. 7A, D, E).

Furthermore, we evaluated STEP and Fyn, and as reported by previous studies [11, 84], our results revealed an increase in both total and nonphosphorylated STEP in the APP/PS1 mice compared to the C57 control mice (Fig. 7F–H). Interestingly, this increase was abrogated following long-term FA supplementation in these mice, as they exhibited levels of this protein comparable to those of C57 control mice. On the other hand, and to our surprise, we found that the level of total Fyn was significantly increased in the APP/PS1 mice compared to the control mice (Fig. 7F, I). However, the level of p-Y416 Fyn was tremendously reduced compared to that in the control mice (Fig. 7F, J). Both the increase in the total and the decrease in the p-Y416 Fyn recovered following 4 months of FA treatment. These data confirm the neuronal experiment results, together suggesting that Aβ triggers the synaptic dysfunction seen as

decreased phosphorylation of NMDA receptors by increasing the level as well as the activity of STEP, which were abrogated by FA treatment.

7. *Ferulic Acid Decreased the Upregulation of STEP in APP/PS1 Mice by Modulating the PP2B/DARPP-32/PP1 Axis*

APP/PS1 mice are an Aβ model of AD, and calcium overload has been reported in the brains of APP/PS1 mice with plaques [85, 86]. Therefore, to investigate the underlying

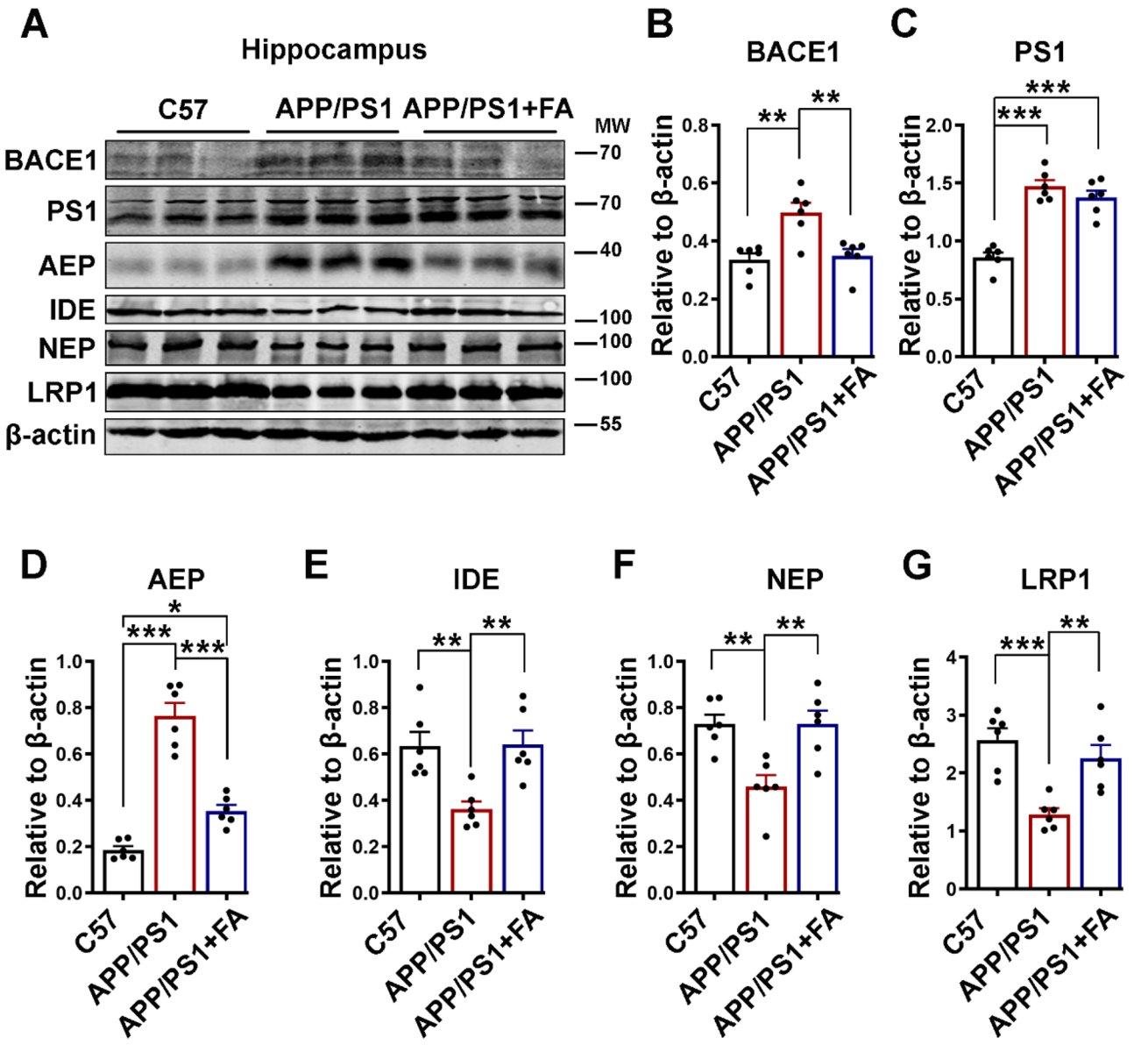


**Fig. 6** FA attenuates the Aβ burden by modulating both production and clearance pathways. **A** The expression levels of BACE1, PS1, AEP, IDE, NEP, and LRP1 in hippocampal lysates of C57 control and APP/PS1 mice with or without long-term FA treatment were evaluated by western blotting. **B**–**G** The quantification of the western blot bands from **A**. β-Actin served as the loading control ($n=6$). The data are presented as the mean ± SEM. *$p<0.05$; **$p<0.01$; and ***$p<0.001$ vs. control or vs. APP/PS1 mice groups

**Fig. 7** FA improves the decrease in p-Y1472 GluN2B by decreasing STEP in APP/PS1 mice. **A** The expression levels of GluN1, GluN2A, GluN2B, and p-Y1472 in hippocampal lysates from C57 control and APP/PS1 mice with or without long-term FA treatment were evaluated by western blotting. **B**–**E** The statistical analysis of western blot bands from **A**. **F** The expression levels of STEP, np-S221, Fyn, and p-Y416 in hippocampal lysates of C57 control and APP/PS1 mice with or without long-term FA treatment were evaluated by western blotting. **G**–**J** Statistical analysis of western blot bands from **F**. β-Actin served as the loading control ($n=6$). The data are presented as the mean ± SEM. ***$p<0.001$ and ****$p<0.0001$ vs. control or vs. APP/PS1 mice groups. p-Y1472, phosphorylated GluN2B at Tyr1472; np-S221, nonphosphorylated STEP at Ser221; p-Y416, phosphorylated Fyn at Tyr416

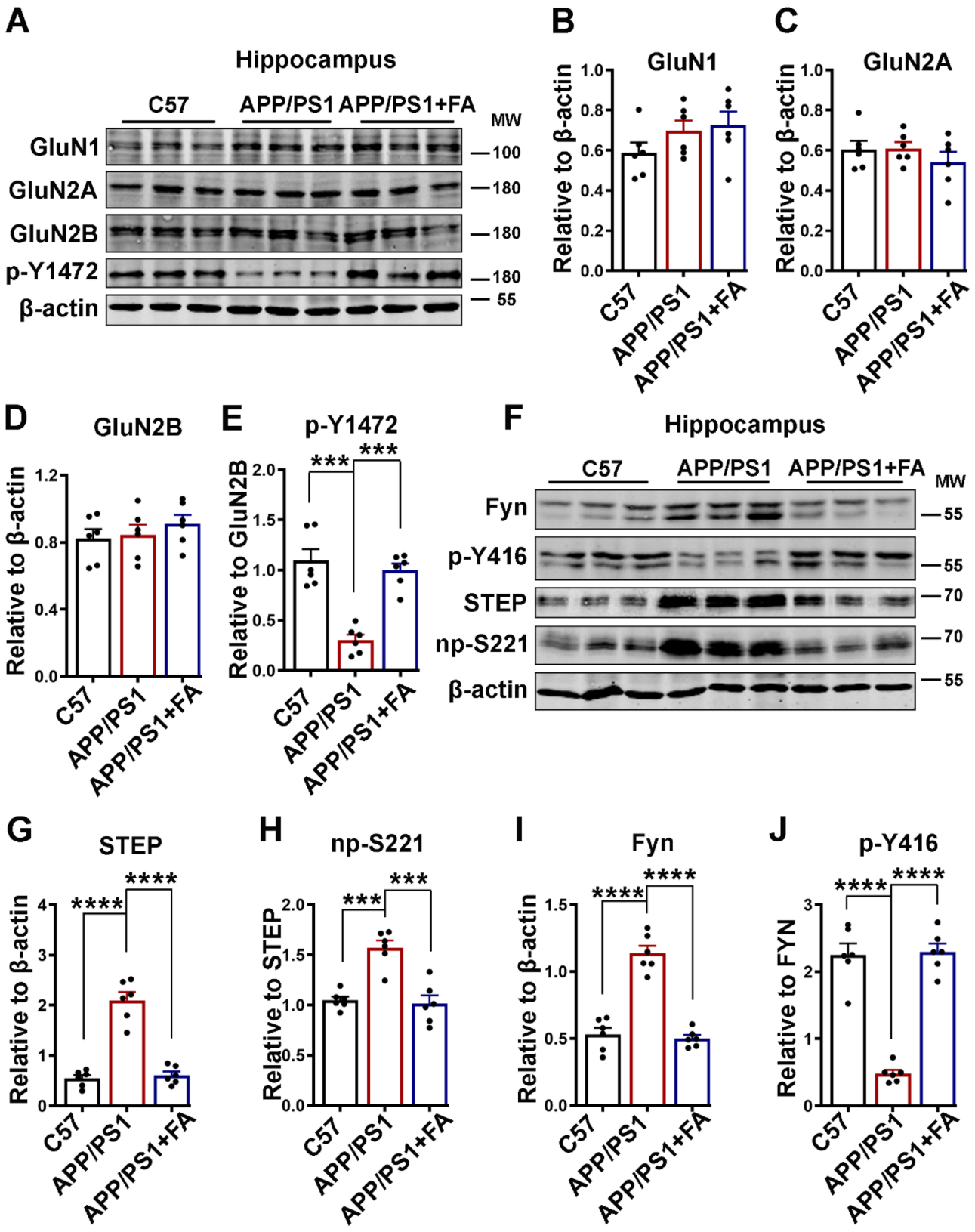
A
Hippocampus
C57
APP/PS1
APP/PS1+FA
MW
GluN1
GluN2A
GluN2B
p-Y1472
β-actin
100
180
180
180
55
B
GluN1
Relative to β-actin
C57
APP/PS1
APP/PS1+FA
C
GluN2A
Relative to β-actin
D
GluN2B
Relative to β-actin
E
p-Y1472
Relative to GluN2B
***
***
F
Hippocampus
Fyn
p-Y416
STEP
np-S221
β-actin
55
55
70
70
55
G
STEP
Relative to β-actin
****
****
H
np-S221
Relative to STEP
***
***
I
Fyn
Relative to β-actin
****
****
J
p-Y416
Relative to FYN
****
****

mechanism of how STEP activity was upregulated in these animals, we evaluated the calcium-linked PP2B/DARPP-32/PP1 axis. We first evaluated the protein levels of total and p-T34 DARPP-32 and p-T320 PP1, and interestingly, similar results to the cell experiment were observed (Fig. 8). The total levels of both DARPP-32 and PP1 were not different among the groups, but p-T34 DARPP-32 and p-T320 PP1 were significantly decreased in the APP/PS1 mice compared to the C57 control mice (Fig. 8A–E). FA supplementation in APP/PS1 improved these changes to control mouse levels, indicating the potential of FA to modulate calcium-related pathways in these animals. To further confirm this speculation, we evaluated the activity of the calcium-dependent phosphatase PP2B. The results revealed increased activity of

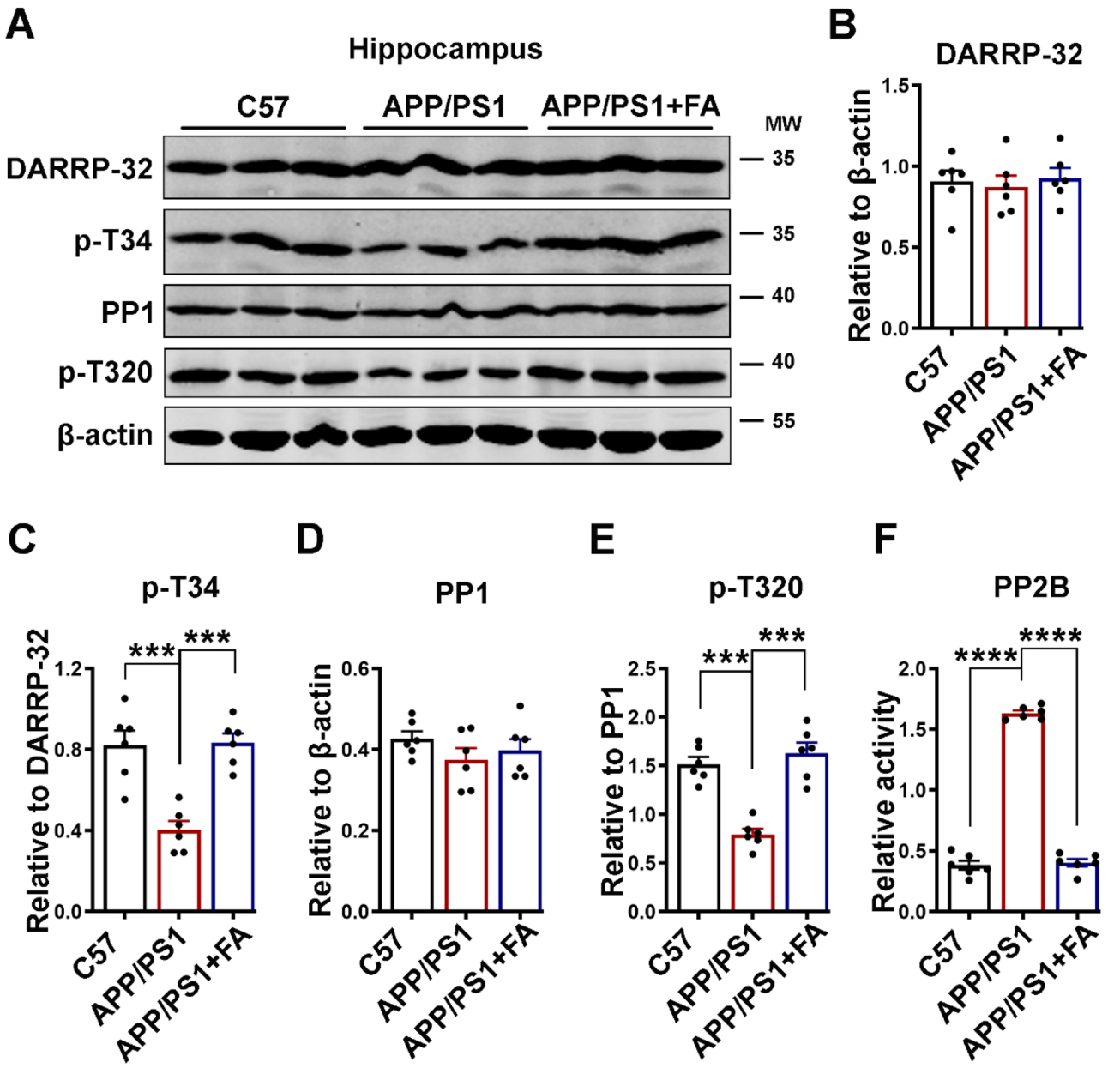


**Fig. 8** FA downregulates STEP by modulating the calcium-related PP2B/DARPP-32/PP1 axis in APP/PS1 mice. **A** The expression levels of DARPP-32, p-T34, PP1, and p-T320 in hippocampal lysates from C57 control and APP/PS1 mice with or without long-term FA treatment were evaluated by western blotting. **B**–**E** Statistical analysis of western blot bands from **A**. β-Actin served as the loading control ($n=6$). **F** Statistical analysis of the PP2B activity test using the PP2B activity kit ($n=6$). The data are presented as the mean ± SEM. ***$p<0.001$ and ****$p<0.0001$ vs. control or vs. APP/PS1 mice groups. p-T34, phosphorylated DARPP-32 at Thr34; p-T320, phosphorylated PP1 at Thr320

this enzyme in the APP/PS1 mice compared to the C57 control and FA-treated APP/PS1 mice (Fig. 8F). These results are an indication that the modulation of the PP2B/DARPP-32/PP1 axis by FA supplementation is at least in part responsible for the downregulated STEP activity, which results in the improvement of the decreased p-Y1472 GluN2B in APP/PS1 mice.

8. *APP/PS1 Mice Exhibited Synaptic Alterations and Neurodegeneration that Were Abrogated by Ferulic Acid Supplementation*

The normal function of synapses is dependent on their integrity, which is maintained by both presynaptic and postsynaptic proteins such as synapsin1 and PSD-95, respectively. The loss of synapses is one of the hallmarks of AD and AD animal models; therefore, we evaluated the synaptic proteins PSD-95 and synapsin1 by western blotting. As observed in our previous report [87] and other studies [88, 89], APP/PS1 mice exhibited significant downregulation of the synaptic proteins PSD-95 and synapsin1 that was abrogated by FA treatment (Fig. 9A–C). Next, we performed Nissl staining, and we found a significant decrease in the number of neurons and cortical thickness in the APP/PS1 mice compared to the C57 control mice and FA-treated APP/PS1 mice (Fig. 9D–F). The results of Golgi staining revealed a decrease in both the total and mushroom-type spines in the APP/PS1 mice that were maintained at the levels seen in C57 control mice following supplementation with FA (Fig. 9G–I). Next, we performed an electrophysiological analysis of hippocampal slices, and as suggested by a decrease in the field excitatory postsynaptic potential (fEPSP) slope and potentiation, the results indicated significantly suppressed LTP at DG-CA3 synapses in the APP/PS1 mouse group compared with the C57 control mouse group (Fig. 9J, K). Interestingly, these changes were prevented by FA administration, suggesting that FA helps in maintaining normal synaptic function. These data together indicate that alterations in both the anatomy and the physiology of synapses occurred in APP/PS1 mice, and these alterations were alleviated by FA supplementation in these mice.

9. *APP/PS1 Mice Exhibited Neuroinflammation that Was Abrogated by Ferulic Acid Supplementation*

Neuroinflammation is an integral and significant part of the pathogenesis of neurodegenerative diseases, including AD. Microglia and astrocytes are major inflammatory cells in the CNS, and together with their secreted cytokines TNF-α and IL-1β, they play a major role in the pathogenesis of AD [90–95]. Therefore, we evaluated the levels of IBA1 (a microglial marker) and GFAP (an astrocyte marker) using western blotting, and the levels of TNF-α and IL-1β were measured using ELISA. The results from our experiments revealed an increase in both IBA1 and GFAP as well as the cytokines TNF-α and IL-1β in the brain hippocampal lysates of the APP/PS1 mice compared to the control mice and the APP/PS1 mice with FA supplementation (Fig. 10A–E). These results confirm that neuroinflammatory processes occur in APP/PS1 mice and that FA can improve these inflammatory changes in these animals.

## Discussion

Alzheimer's disease is a devastating neurodegenerative disease, the most common, that has seen an exponentially increased prevalence due to medical progress that has resulted in increased longevity and thus increased aging of the global population. Current evidence supports the view that Aβ is the trigger that leads to the cascade that results in tau pathology, neuroinflammation, and the subsequent neuronal cell death that translates to neurodegeneration and synapse loss, finally culminating in cognitive decline [95–97]. Despite decades of research in the field of AD, no cure exists for this debilitating disease, and many of the Aβ- and tau-targeted therapies have failed [21, 22, 98, 99], thus leaving clinicians with limited management strategies. With increasing age, the CNS becomes more susceptible to oxidative stress, widely affecting proteins, lipids, and nucleic acids [100]. Clear evidence suggests that oxidative stress is centrally involved in AD and that oxidative stress can trigger an increase in intracellular calcium influx [31]. In the present study, we provide evidence that the antioxidant and $Ca^{2+}$ chelator FA ameliorates the Aβ-induced molecular, physiological, and behavioral alterations that are observed in AD.

Increased Aβ production is observed in the early stage of AD [101], and this is associated with synaptic dysfunction and cognition deficits even before overt toxicity [56, 102]. Synaptic plasticity is the basic process for memory formation, and NMDARs play a crucial role in synaptic plasticity and thus learning and memory [1–3]. Here, we found that Aβ induced a significant decrease in both the total and p-Y1472 GluN2B subunit of NMDAR, and these changes were absent from the group of neurons pretreated with FA before Aβ incubation. Moreover, 4 months of treatment with FA prevented the observed loss of p-Y1472 GluN2B in APP/PS1 mice. It has been demonstrated that GluN2B is the most prominent tyrosine-phosphorylated protein within PSDs [103], and its phosphorylation is upregulated during LTP in the CA1 hippocampus [104]. The synaptic expression of NMDARs is significantly regulated by their phosphorylation [105], and the activity-dependent subunit-specific phosphorylation of NMDARs has a significant impact on their synaptic localization and function [106, 107]. Thus, our

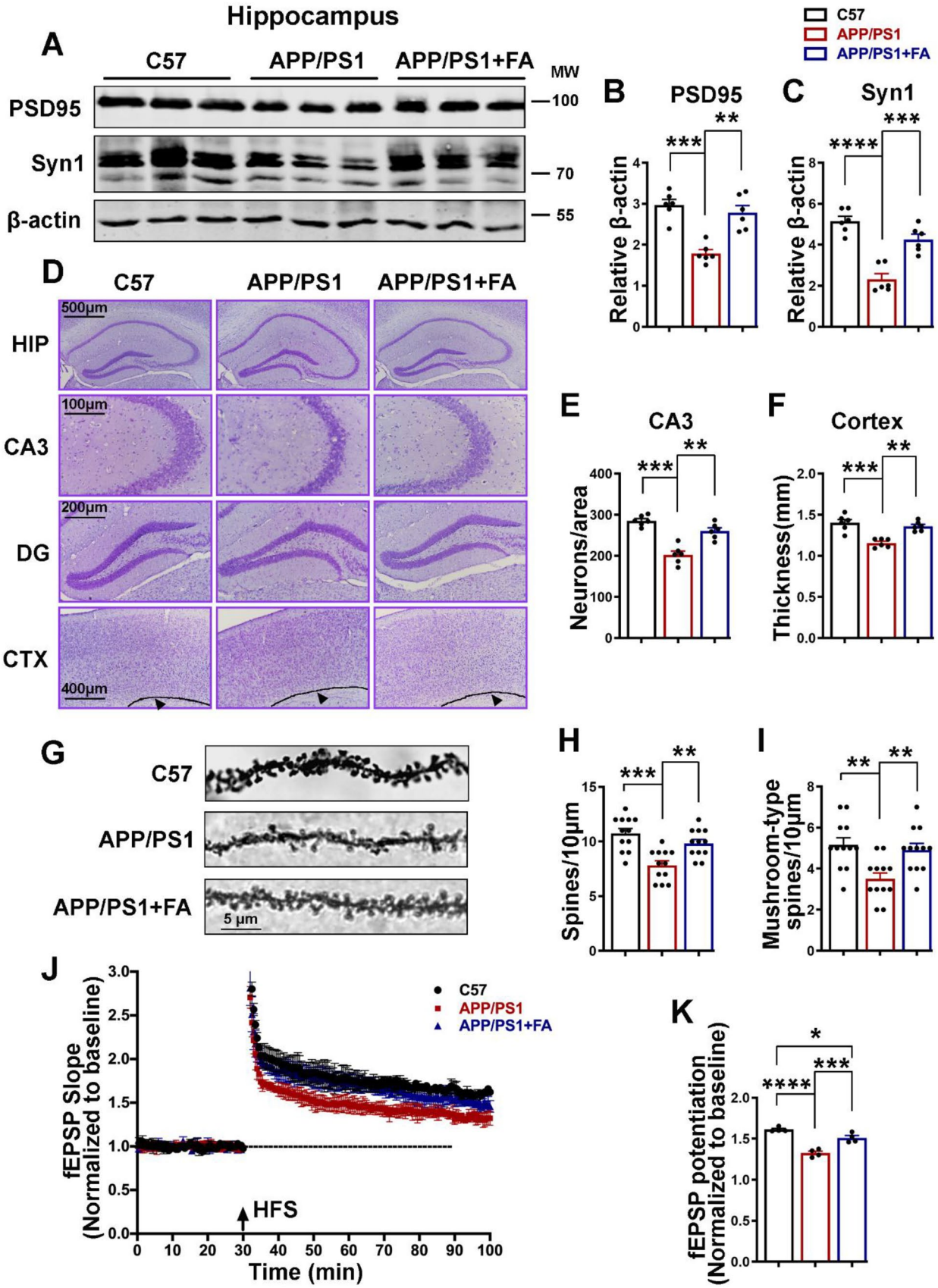
Hippocampus
A
C57
APP/PS1
APP/PS1+FA
MW
PSD95
Syn1
β-actin
100
70
55
B
PSD95
Relative β-actin
C
Syn1
Relative β-actin
D
HIP
CA3
DG
CTX
500μm
100μm
200μm
400μm
E
CA3
Neurons/area
F
Cortex
Thickness(mm)
G
5 μm
H
Spines/10μm
I
Mushroom-type spines/10μm
J
fEPSP Slope (Normalized to baseline)
HFS
Time (min)
K
fEPSP potentiation (Normalized to baseline)

◂**Fig. 9** Long-term FA treatment prevents synaptic loss and neurodegeneration and improves LTP in APP/PS1 mice. **A** The expression levels of PSD-95 and Synapsin1 from hippocampal lysates from C57 control and APP/PS1 mice with or without long-term FA treatment were evaluated by western blotting. **B**, **C** Statistical analysis of western blot bands of PSD-95 and Synapsin1 from **A**. β-Actin served as the loading control ($n=6$). **D–F** Nissl staining results (scale bars = 100, 200, 400, and 500 μm, $n=6$; 3 mice per group and 2 images per mouse). **D** Representative micrographs of the Nissl staining experiment. **E** The number of neurons per area. **F** Thickness (mm) of the cortex. **G–I** Golgi staining results. **G** Representative micrographs of the Golgi staining experiment (scale bar = 5 μm, $n=12$ images analyzed per group, 3 mice per group, and 4 dendrites per mouse). **H** Total spine number per 10 μm area. **I** The mushroom-type spines per 10 μm area. **J**, **K** LTP at DG-CA3 synapses was measured in C57 control and APP/PS1 mice with or without long-term FA treatment ($n=4$ mice per group, 3 brain slices per mouse). **J** The normalized fEPSP slope. **K** Normalized fEPSP potentiation. The data are presented as the mean ± SEM. *$p<0.05$; **$p<0.01$; ***$p<0.001$; and ****$p<0.0001$ vs. control or vs. APP/PS1 mice groups

results indicate the role of FA in preserving normal synaptic function and therefore learning and memory. Interestingly, the decrease in p-Y1472 GluN2B correlates with an increase in np-S221 STEP (active) and a decrease in p-Y416 Fyn (active) in both neuronal cultures and APP/PS1 mice that were rescued by FA treatment. Unexpectedly, we observed an increase in the level of total Fyn in the APP/PS1 mice, possibly indicating a compensatory mechanism from the mouse body in response to the decreased level of active Fyn. Moreover, in accordance with previous reports [12, 108], an increase in the total level of STEP was also observed in the APP/PS1 mice. STEP is the main phosphatase that dephosphorylates GluN2B at Tyr1472 [25] as well as Fyn at both Tyr416 [109] and Tyr420 [110]. Interestingly, Fyn is the main kinase that phosphorylates GluN2B at Tyr1472, implying that the decrease in p-Y1472 GluN2B could be the result of direct dephosphorylation by STEP as well as indirect decreased phosphorylation by Fyn. This indicates that STEP is one of the major pathways of Aβ-mediated synaptic damage in AD, and FA might prevent these changes by decreasing STEP.

It was previously reported that NMDA receptor endocytosis requires the activation of α7nAChRs, PP2B, and STEP [25]. In line with this, our results revealed an upregulated activity of PP2B and a decrease in p-T34 DARPP-32 (inhibitor of PP1) and p-T320 PP1 in both Aβ-treated neurons and APP/PS1 mice, which was correlated with an increased intracellular $Ca^{2+}$ in the neurons. These results indicate the activation of PP1 via the inactivation of DARPP-32 due to increased PP2B activity as a result of intracellular $Ca^{2+}$ influx. Interestingly, PP1 not only can undergo autodephosphorylation but also can transdephosphorylate other PP1 molecules [111, 112]. Therefore, the removal of DARPP-32 inhibition of PP1 might trigger PP1 autodephosphorylation, resulting in a decrease in p-T320 PP1. Interestingly, FA treatment attenuated the intracellular $Ca^{2+}$ increase in neuronal cells and reduced PP2B activity to levels comparable to those of the control in both neurons and APP/PS1 mice. FA is reported to be an extracellular $Ca^{2+}$ ion chelator and a blocker of N-type and P/Q-type $Ca^{2+}$ channels [46], which might at least in part explain this result, but further analysis is needed for confirmation. Together, these data suggest that FA improves p-Y1472 GluN2B loss by downregulating STEP, possibly by decreasing the intracellular $Ca^{2+}$ increase induced by Aβ.

Precise communication between presynaptic and postsynaptic elements is required for normal synaptic function [113, 114]. A loss of dendritic synaptic plasticity occurs in the brains of AD patients, and this constitutes a key neurobiological basis of dementia [115, 116]. Our data revealed that PSD-95 and synapsin1 were downregulated in Aβ-treated neurons as well as in APP/S1 mice. Nissl staining also revealed a decrease in the number of neurons in the CA3 region of the hippocampus and a reduction in the thickness of the cortical area, suggesting neurodegeneration, in the APP/PS1 mice. Moreover, a decrease in both total and mushroom-type spines and suppressed LTP were also reported in APP/PS1 mice. Interestingly, all these alterations were abrogated by FA supplementation. PSD-95 is a scaffolding protein, the major component of PSD, that functions as a PSD organizer and is central to glutamatergic synaptic signaling [117]. PSD-95 is reported to stabilize the surface expression of GluN2B-containing NMDARs by its direct interaction with the GluN2B PDZ ligand and by triggering STEP ubiquitination and degradation [5, 9], resulting in increased GluN2B phosphorylation during LTP [104]. PSD-95 also interacts with cysteine-rich PDZ-binding protein and forms a linkage with the neuronal cytoskeleton to regulate dendritic arborization and spine number [118]. PSD-95 forms a ternary complex with GluN2B and nNOS [119] and can also indirectly regulate the dendritic spine AMPAR content, and all these processes are essential for basal synaptic transmission and LTP establishment [120]. Interestingly, the knockdown of PSD-95, PSD-93, and SAP-102 reduces NMDAR- and AMPAR-regulated synaptic transmission and alters both the size and structure of PSD [121], while acute depletion of PSD-95 leads to hippocampal neuron death via the activation of a calcium-dependent αCaMKII transduction pathway [122]. Moreover, neurons lacking PSD-95 are more prone to NMDAR-mediated excitotoxicity, resulting in neuronal damage and neurological impairment [123]. A recent study also demonstrated that PSD-95 plays a protective role against Aβ toxicity in synapses [124], which implies that a decrease in synaptic PSD-95 might suggest synaptic vulnerability to Aβ in AD. Interestingly, the main mechanism mediating excitotoxic PSD-95 downregulation in neurons is believed to be $Ca^{2+}$ influx-induced calpain

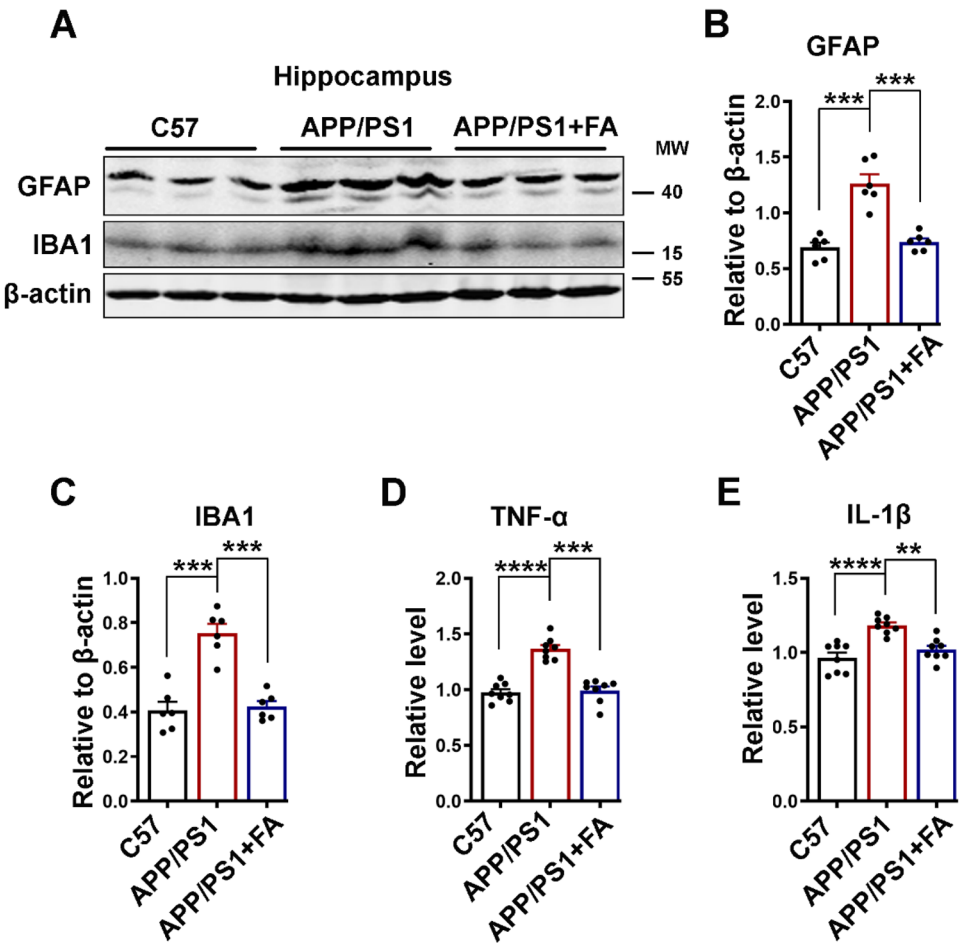


**Fig. 10** Long-term FA treatment improves neuroinflammation in APP/PS1 mice. **A** The expression levels of GFAP and IBA1 in hippocampal lysates of C57 control and APP/PS1 mice with or without long-term FA treatment were evaluated by western blotting. **B**, **C** Statistical analysis of western blot bands of GFAP and IBA1 from **A**. β-Actin served as the loading control ($n=6$). **D**, **E** Statistical analysis of TNF-α and IL-1β ELISA results ($n=8$; 4 mice per group and 3 independent experiments). The data are presented as the mean ± SEM. $^{**}p<0.01$; $^{***}p<0.001$; and $^{****}p<0.0001$ vs. control or vs. APP/PS1 mice groups

activation [125]. The presynaptic protein synapsin1 also plays an important role in neurogenesis, synapse formation, and synaptic transmission [126], suggesting its important role in learning and memory. A recent study also revealed that mushroom-type spines are more liable to respond to dynamic changes in synaptic transmission, and their content correlates more with synaptic strength [127]. It is clear that oxidative stress is implicated in AD and that oxidative stress can trigger an increase in intracellular $Ca^{2+}$ [31]. Altogether, these results suggest that the antioxidative and $Ca^{2+}$ chelating abilities of FA might play an important role in preventing the loss of PSD-95 and the increase in STEP observed in Aβ-treated neurons and APP/PS1 mice, thereby maintaining normal neuronal function and thus learning and memory.

Aβ is the trigger for the pathological cascade that leads to AD, and APP/PS1 mice are an AD model that overproduces Aβ. In line with previous studies [36, 42, 128], we found that long-term FA supplementation helps reduce the level of Aβ in these mice, which in part might be the cause of the improvements in the alterations observed in these mice. BACE1, the rate-limiting enzyme in amyloidogenic APP processing and the age-related decrease in Aβ clearance both contribute to Aβ accumulation in AD [32, 74–77]. Interestingly, FA influences both the Aβ production and clearance pathways, leading to decreased Aβ levels. In accordance with other reports [41, 42], our results revealed a decrease in the protein level of BACE1. The expression of this enzyme was also reported to be mediated by a cascade related to increased intracellular $Ca^{2+}$ that activates calpain, which activates CDK5 via p35 to p25 conversion (activation), which in turn activates STAT3, a BACE1 transcription factor, or another calcium-related BACE1 transcription factor, NFAT1 [31]. Recently, the delta secretase AEP was found to be involved in the amyloidogenic processing of APP [78–81]. The AEP-truncated APP fragment (APP 586–695) binds to the CEBPB transcription factor and upregulates the expression of AD-related genes and AD pathogenesis [80]. The blockage of AEP cleavage of APP, as well as antibody-mediated clearance of APP 586–695, ameliorates Aβ pathology and cognitive impairments [80]. AEP also cleaves Tau, producing Tau 1–368, which activates STAT1 and increases BACE1 production, and together with APP 586–695 mediates AD [79]. Again, AEP was shown to cleave BACE1 at N294 and increase its protease activity, thereby promoting Aβ production [78]. Interestingly, AEP can be activated by DOPAL, a highly toxic and oxidative dopamine metabolite

[129], as well as by DOPEGAL, a norepinephrine derivative that is upregulated due to increased free radicals [130], indicating that AEP could be activated under increased oxidative stress. Calcium overload can also induce oxidative stress by impairing normal mitochondrial function as well as by increasing Aβ production. Interestingly, calcium overload was observed in approximately 20% of neurites in APP/PS1 mice with cortical plaques, compared to less than 5% in wild-type mice, PS1 mutant mice, or younger APP/PS1 mice without plaques [85]. Our results showed increased Aβ plaques and AEP protein levels in APP/PS1 mice that were significantly reduced following FA supplementation. Altogether, these results suggest that FA ameliorates the AEP-mediated increase in BACE1 activation and amyloidogenic processing of APP and thus the Aβ burden observed in APP/PS1 mice, probably by decreasing oxidative stress and $Ca^{2+}$ overload. Among a multitude of proteases that degrade Aβ, NEP [131, 132] and IDE [133] play a significant role in extracellular and intracellular Aβ degradation. IDE can be found in almost all cellular compartments, in extracellular vesicles, in the blood, and in cerebrospinal fluid, and it can proteolytically degrade β-structure-forming peptides associated with neurodegeneration [134]. IDE regulates the Aβ level in vivo [135] and is found to decrease with age and in the early stage of AD [133]. Moreover, polymorphisms in the genes encoding IDE and NEP were found to be associated with a higher risk of AD [136, 137], and conformational changes in these enzymes might be relevant to AD pathogenesis [138]. LRP1 is another protein related to Aβ clearance and is normally reduced with increasing age but is further decreased in AD [139–141], and both pharmacologic and genetic inhibition of LRP1 in pericytes were shown to lead to Aβ accumulation [142]. Furthermore, selective deletion of the LRP1 gene in the brain endothelium resulted in decreased plasma Aβ and increased brain Aβ, exacerbating memory deficits in 5xFAD mice [143]. By suppressing cyclophilin-A activation, endothelial LRP1 was also shown to protect the brain from blood–brain barrier breakage and thus against neurodegeneration [144]. Interestingly, IDE, NEP, and LRP1 were found to be decreased in APP/PS1 mice, and FA treatment rescued these proteins to the level of control mice, indicating that FA reduced the Aβ burden by preventing the loss of these proteins in APP/PS1 mice.

Clear evidence indicates that neuroinflammation is a key player in the etiopathogenesis of Alzheimer's disease [145–148]. Moreover, the spatiotemporal relationship of Aβ, tau, and glial cells is a conducive environment where Aβ and glial cells trigger neuroinflammation, and in turn, neuroinflammation was reported to influence the generation of Aβ [149]. Increased TNF-α is said to be centrally involved in AD pathogenesis [90–92], while IL-1β inhibits LTP in the hippocampus [150]. TNF-α functions in vivo as a gliotransmitter that regulates synaptic function in the brain [151] and has also been demonstrated to control synaptic strength and directly affect glutamate transmission [91, 152]. Many studies have reported the ameliorative effect of FA on neuroinflammation, whereby FA was found to decrease TNF-α and IL-1β, oxidative stress, and neurotoxicity [35–37, 44, 153]. FA also abrogated the Aβ-induced activation of astrocytes, which release free radicals and proinflammatory cytokines such as IL-1β [44, 128]. Our results revealed an increase in GFAP, IBA1, TNF-α, and IL-1β that was decreased following FA treatment, further elucidating the role of FA in modulating neuroinflammation. All the pathological processes discussed thus far come together and manifest as cognitive, behavioral, learning, and memory impairments in AD patients and AD animal models. Our results from a battery of behavioral tests revealed hyperactivity, anxiety, cognition, learning, and memory impairments in APP/PS1 mice, all of which were improved following FA treatment. This is consistent with previous studies that reported that long-term administration of FA protected rodents from Aβ-induced cognitive and behavioral deficits [35–37, 42, 44, 128, 154, 155]. Interestingly, previous studies showed that FA does not affect the normal physiology and behavior of WT mice [35, 37, 42], indicating that the improvement in behavioral and cognitive alterations exhibited by FA-treated APP/PS1 mice is a response to these changes.

The data from this study strongly support the deleterious effects of Aβ and the protective role of FA against these effects. However, further studies will be needed to clarify the mechanisms of the Aβ-induced decrease in total GluN2B. It would also be interesting to investigate whether the dephosphorylation of GluN2B triggers its ubiquitination and degradation. It should be noted that our study has some limitations, including a lack of proper controls (no scrambled peptide control for Aβ treatment in the cell experiment and no C57 + FA control in the animal experiment), and the immunofluorescence experiment of total and p-Y1472 GluN2B was performed in different sets of neurons. These might dampen the rigor of our experimental results and therefore will be considered in our future works.

## Conclusion

Here, we showed that Aβ induces the activation of the $Ca^{2+}$-related PP2B/DARPP-32/PP1/STEP axis to impair normal synaptic functions, and these changes were abrogated by FA treatment in both neurons and APP/PS1 mice. FA also prevented the increased Aβ burden in these animals by modulating both Aβ production and clearance pathways and improving neuroinflammation. This study provides insight into the use of FA as a potential disease-modifying agent that improves synaptic functions possibly by modulating oxidative stress and $Ca^{2+}$-related pathways involving STEP, Fyn, GluN2B, PSD-95, and BACE1 in AD.

**Abbreviations** 3×Tg: Triple transgenic; aCSF: Artificial cerebrospinal fluid; AD: Alzheimer's disease; AEP: Asparagine endopeptidase; AMPA: α-Amino-3-hydroxy-5-methyl-4-isoxazole propionic acid; AMPARs: α-Amino-3-hydroxy-5-methyl-4-isoxazole propionic acid receptors; APOE-4: Apolipoprotein E-4; APP: Amyloid precursor protein; Aβ: Amyloid-beta; BACE1: Beta APP cleaving enzyme 1; BCA: Bicinchoninic acid; CA1: Cornu ammonis area 1; CA3: Cornu ammonis area 3; CaMKII: Calcium calmodulin-dependent protein kinase II; CDK5: C-dependent kinase 5; CEBPB: CCAAT/enhancer-binding protein beta; CNS: Central nervous system; CRIPT: Cysteine-rich PDZ-binding protein; CXA: Chloroform, xylene, alcohol; DARPP-32: Dopamine- and cyclic-AMP-regulated phosphoprotein of molecular weight 32,000; DG: Dentate gyrus; DMEM/F12: Dulbecco's modified eagle medium/nutrient mixture F-12; DMSO: Dimethyl sulfoxide; DMTs: Disease-modifying therapies; DOPAL: 3,4-Dihydroxy-benzeneacetaldehyde; DOPEGAL: 3,4-Dihydroxyphenylglycolaldehyde; ELISA: Enzyme-linked immunosorbent assay; ERK1/2: Extracellular signal-regulated protein kinases 1 and 2; FA: Ferulic acid; fEPSP: Field excitatory postsynaptic potential; GFAP: Glial fibrillary acidic protein; GSK-3β: Glucose synthase kinase 3β; HFS: High-frequency stimulation; IBA1: Ionized calcium-binding adaptor molecule 1; IDE: Insulin-degrading enzyme; IL-1β: Interleukin 1β; LRP1: Low-density lipoprotein receptor-related protein 1; LTP: Long-term potentiation; MAGUK: Membrane-associated guanylate kinase; MWM: Morris water maze; NEP: Neprilysin; NFAT1: Nuclear factor of activated T cells 1; NFTs: Neurofibrillary tangles; NMDA: *N*-Methyl-D-aspartate; NMDARs: *N*-Methyl-D-aspartate receptors; nNOS: Neuronal nitric oxide synthase; NOR: Novel object recognition; OFT: Open field test; PBS: Phosphate-buffered saline; PDP3: PP1-disrupting peptide 3; PKA: Protein kinase A; PP1: Protein phosphatase 1; PP2A: Protein phosphatase 2A; PP2B: Protein phosphatase 2B; PS1: Presenilin-1; PSD-95: Postsynaptic density 95; Pyk2: Proline-rich tyrosine kinase 2; SAMP8: Senescence accelerated mouse-prone 8; SDS-PAGE: Sodium dodecyl sulfate–polyacrylamide gel electrophoresis; STAT1: Signal transducers and activators of transcription 1; STAT3: Signal transducers and activators of transcription 3; STEP: Striatal-enriched protein tyrosine phosphatase; TBS: Tris-buffered saline; TNF-α: Tumor necrosis factor α; UPS: Ubiquitin-proteasome system; WT: Wild type; α7nAChRs: α7 Nicotinic acetylcholine receptors

**Supplementary Information** The online version contains supplementary material available at https://doi.org/10.1007/s13311-023-01356-6.

**Acknowledgements** The authors thank the Medical Subcenter of the HUST Analytical & Testing Center for data acquisition.

**Required Author Forms** Disclosure forms provided by the authors are available with the online version of this article.

**Funding** This work is supported by grants from the National Natural Science Foundation of China (82150410454, 92049107, 31929002, and 82071440), the Innovative Research Groups of the National Natural Science Foundation of China (81721005), and the Academic Frontier Youth Team Project to Xiaochuan Wang from Huazhong University of Science and Technology, as well as the Science, Technology and Innovation Commission of Shenzhen Municipality (JCYJ20210324141405014) and the Guangdong Basic and Applied Basic Research Foundation (2020B1515120017).

**Data Availability** All data used in this study are available from the corresponding authors upon reasonable request.

## Declarations

**Ethics Approval** All animal handling and uses were performed according to the protocol approved by the Institutional Animal Care and Use Committee of Tongji Medical School of Huazhong University of Science and Technology.

**Consent for Publication** All authors read and approved the final manuscript.

**Conflict of Interest** The authors declare no competing interests.

## References

1. Bliss TV, Collingridge GL. A synaptic model of memory: long-term potentiation in the hippocampus. Nature. 1993;361:31–9.
2. Sattler R, Xiong Z, Lu WY, MacDonald JF, Tymianski M. Distinct roles of synaptic and extrasynaptic NMDA receptors in excitotoxicity. J Neurosci. 2000;20:22–33.
3. Hardingham GE, Fukunaga Y, Bading H. Extrasynaptic NMDARs oppose synaptic NMDARs by triggering CREB shut-off and cell death pathways. Nat Neurosci. 2002;5:405–14.
4. Chatterjee M, Kwon J, Benedict J, Kamceva M, Kurup P, Lombroso PJ. STEP inhibition prevents Aβ-mediated damage in dendritic complexity and spine density in Alzheimer's disease. Exp Brain Res. 2021;239:881–90.
5. Won S, Roche KW. Regulation of glutamate receptors by striatal-enriched tyrosine phosphatase 61 (STEP(61)). J Physiol. 2021;599:443–51.
6. Jang SS, Royston SE, Xu J, Cavaretta JP, Vest MO, Lee KY, et al. Regulation of STEP61 and tyrosine-phosphorylation of NMDA and AMPA receptors during homeostatic synaptic plasticity. Mol Brain. 2015;8:55.
7. Won S, Incontro S, Li Y, Nicoll RA, Roche KW. The STEP(61) interactome reveals subunit-specific AMPA receptor binding and synaptic regulation. Proc Natl Acad Sci U S A. 2019;116:8028–37.
8. Lombroso PJ, Murdoch G, Lerner M. Molecular characterization of a protein-tyrosine-phosphatase enriched in striatum. Proc Natl Acad Sci U S A. 1991;88:7242–6.
9. Won S, Incontro S, Nicoll RA, Roche KW. PSD-95 stabilizes NMDA receptors by inducing the degradation of STEP61. Proc Natl Acad Sci U S A. 2016;113:E4736–44.
10. Pelkey KA, Askalan R, Paul S, Kalia LV, Nguyen TH, Pitcher GM, et al. Tyrosine phosphatase STEP is a tonic brake on induction of long-term potentiation. Neuron. 2002;34:127–38.
11. Mahaman YAR, Huang F, Embaye KS, Wang X, Zhu F. The implication of STEP in synaptic Plasticity and cognitive impairments in Alzheimer's Disease and other neurological disorders. Front Cell Dev Biol. 2021;9:680118.
12. Kurup P, Zhang Y, Xu J, Venkitaramani DV, Haroutunian V, Greengard P, et al. Abeta-mediated NMDA receptor endocytosis in Alzheimer's disease involves ubiquitination of the tyrosine phosphatase STEP61. J Neurosci. 2010;30:5948–57.
13. Zhang Y, Kurup P, Xu J, Carty N, Fernandez SM, Nygaard HB, et al. Genetic reduction of striatal-enriched tyrosine phosphatase (STEP) reverses cognitive and cellular deficits in an Alzheimer's disease mouse model. Proc Natl Acad Sci U S A. 2010;107:19014–9.
14. Wang JZ, Wang ZH, Tian Q. Tau hyperphosphorylation induces apoptotic escape and triggers neurodegeneration in Alzheimer's disease. Neurosci Bull. 2014;30:359–66.
15. As A. 2013 Alzheimer's disease facts and figures. Alzheimers Dement. 2013;9:208–45.
16. Rosenberg RN, Lambracht-Washington D, Yu G, Xia W. Genomics of Alzheimer disease: a Review. JAMA Neurol. 2016;73:867–74.

17. Reitz C, Brayne C, Mayeux R. Epidemiology of Alzheimer disease. Nat Rev Neurol. 2011;7:137–52.
18. Li YM, Xu M, Lai MT, Huang Q, Castro JL, DiMuzio-Mower J, et al. Photoactivated gamma-secretase inhibitors directed to the active site covalently label presenilin 1. Nature. 2000;405:689–94.
19. Terry RD, Masliah E, Salmon DP, Butters N, DeTeresa R, Hill R, et al. Physical basis of cognitive alterations in Alzheimer's disease: synapse loss is the major correlate of cognitive impairment. Ann Neurol. 1991;30:572–80.
20. Knobloch M, Mansuy IM. Dendritic spine loss and synaptic alterations in Alzheimer's disease. Mol Neurobiol. 2008;37:73–82.
21. Extance A. Alzheimer's failure raises questions about disease-modifying strategies. Nat Rev Drug Discov. 2010;9:749–51.
22. Rinne JO, Brooks DJ, Rossor MN, Fox NC, Bullock R, Klunk WE, et al. 11C-PiB PET assessment of change in fibrillar amyloid-beta load in patients with Alzheimer's disease treated with bapineuzumab: a phase 2, double-blind, placebo-controlled, ascending-dose study. Lancet Neurol. 2010;9:363–72.
23. Cummings J, Lee G, Ritter A, Sabbagh M, Zhong K. Alzheimer's disease drug development pipeline: 2020. Alzheimer's Dement Transl Res Clin Interv. 2020;6:e12050.
24. Dewachter I, Filipkowski RK, Priller C, Ris L, Neyton J, Croes S, et al. Deregulation of NMDA-receptor function and downstream signaling in APP[V717I] transgenic mice. Neurobiol Aging. 2009;30:241–56.
25. Snyder EM, Nong Y, Almeida CG, Paul S, Moran T, Choi EY, et al. Regulation of NMDA receptor trafficking by amyloid-beta. Nat Neurosci. 2005;8:1051–8.
26. Dineley KT, Westerman M, Bui D, Bell K, Ashe KH, Sweatt JD. Beta-amyloid activates the mitogen-activated protein kinase cascade via hippocampal alpha7 nicotinic acetylcholine receptors: In vitro and in vivo mechanisms related to Alzheimer's disease. J Neurosci. 2001;21:4125–33.
27. Stevens TR, Krueger SR, Fitzsimonds RM, Picciotto MR. Neuroprotection by nicotine in mouse primary cortical cultures involves activation of calcineurin and L-type calcium channel inactivation. J Neurosci. 2003;23:10093–9.
28. Lacor PN, Buniel MC, Chang L, Fernandez SJ, Gong Y, Viola KL, et al. Synaptic targeting by Alzheimer's-related amyloid beta oligomers. J Neurosci. 2004;24:10191–200.
29. Lucić V, Greif GJ, Kennedy MB. Detailed state model of CaMKII activation and autophosphorylation. Eur Biophys J. 2008;38:83–98.
30. Feng Y, Xia Y, Yu G, Shu X, Ge H, Zeng K, et al. Cleavage of GSK-3beta by calpain counteracts the inhibitory effect of Ser9 phosphorylation on GSK-3beta activity induced by H(2)O(2). J Neurochem. 2013;126:234–42.
31. Mahaman YAR, Huang F, Kessete Afewerky H, Maibouge TMS, Ghose B, Wang X. Involvement of calpain in the neuropathogenesis of Alzheimer's disease. Med Res Rev. 2019;39:608–30.
32. Chami L, Checler F. BACE1 is at the crossroad of a toxic vicious cycle involving cellular stress and β-amyloid production in Alzheimer's disease. Mol Neurodegener. 2012;7:52.
33. Xu J, Chatterjee M, Baguley TD, Brouillette J, Kurup P, Ghosh D, et al. Inhibitor of the tyrosine phosphatase STEP reverses cognitive deficits in a mouse model of Alzheimer's disease. PLoS Biol. 2014;12:e1001923.
34. Nabavi SF, Devi KP, Malar DS, Sureda A, Daglia M, Nabavi SM. Ferulic acid and Alzheimer's disease: promises and pitfalls. Mini Rev Med Chem. 2015;15:776–88.
35. Mori T, Koyama N, Tan J, Segawa T, Maeda M, Town T. Combination therapy with octyl gallate and ferulic acid improves cognition and neurodegeneration in a transgenic mouse model of Alzheimer's disease. J Biol Chem. 2017;292:11310–25.
36. Wang H, Sun X, Zhang N, Ji Z, Ma Z, Fu Q, et al. Ferulic acid attenuates diabetes-induced cognitive impairment in rats via regulation of PTP1B and insulin signaling pathway. Physiol Behav. 2017;182:93–100.
37. Mori T, Koyama N, Tan J, Segawa T, Maeda M, Town T. Combined treatment with the phenolics (-)-epigallocatechin-3-gallate and ferulic acid improves cognition and reduces Alzheimer-like pathology in mice. J Biol Chem. 2019;294:2714–31.
38. Ghosh S, Basak P, Dutta S, Chowdhury S, Sil PC. New insights into the ameliorative effects of ferulic acid in pathophysiological conditions. Food Chem Toxicol. 2017;103:41–55.
39. Ghosh S, Chowdhury S, Sarkar P, Sil PC. Ameliorative role of ferulic acid against diabetes associated oxidative stress induced spleen damage. Food Chem Toxicol. 2018;118:272–86.
40. Kim YJ, Jeong SJ, Seo CS, Lim HS, Sohn E, Yun J, et al. Simultaneous determination of the traditional herbal formula Ukgansan and the in vitro antioxidant activity of ferulic acid as an active compound. Molecules (Basel, Switzerland). 2018;23.
41. Meng G, Meng X, Ma X, Zhang G, Hu X, Jin A, et al. Application of ferulic acid for Alzheimer's disease: combination of text mining and experimental validation. Front Neuroinform. 2018;12:31.
42. Mori T, Koyama N, Guillot-Sestier MV, Tan J, Town T. Ferulic acid is a nutraceutical beta-secretase modulator that improves behavioral impairment and alzheimer-like pathology in transgenic mice. PLoS ONE. 2013;8:e55774.
43. Ono K, Hirohata M, Yamada M. Ferulic acid destabilizes preformed beta-amyloid fibrils in vitro. Biochem Biophys Res Commun. 2005;336:444–9.
44. Yan JJ, Cho JY, Kim HS, Kim KL, Jung JS, Huh SO, et al. Protection against beta-amyloid peptide toxicity in vivo with long-term administration of ferulic acid. Br J Pharmacol. 2001;133:89–96.
45. Wang NY, Li JN, Liu WL, Huang Q, Li WX, Tan YH, et al. Ferulic acid ameliorates Alzheimer's disease-like pathology and repairs cognitive decline by preventing capillary hypofunction in APP/PS1 mice. Neurotherapeutics. 2021;18:1064–80.
46. Lin TY, Lu CW, Huang SK, Wang SJ. Ferulic acid suppresses glutamate release through inhibition of voltage-dependent calcium entry in rat cerebrocortical nerve terminals. J Med Food. 2013;16:112–9.
47. Li D, Rui YX, Guo SD, Luan F, Liu R, Zeng N. Ferulic acid: a review of its pharmacology, pharmacokinetics and derivatives. Life Sci. 2021;284:119921.
48. Li Y, Liu C, Zhang Y, Mi S, Wang N. Pharmacokinetics of ferulic acid and potential interactions with Honghua and clopidogrel in rats. J Ethnopharmacol. 2011;137:562–7.
49. Zhao Z, Egashira Y, Sanada H. Ferulic acid is quickly absorbed from rat stomach as the free form and then conjugated mainly in liver. J Nutr. 2004;134:3083–8.
50. Wu K, Wang ZZ, Liu D, Qi XR. Pharmacokinetics, brain distribution, release and blood-brain barrier transport of Shunaoxin pills. J Ethnopharmacol. 2014;151:1133–40.
51. Yan N, Tang Z, Xu Y, Li X, Wang Q. Pharmacokinetic study of ferulic acid following transdermal or intragastric administration in rats. AAPS PharmSciTech. 2020;21:169.
52. Xia T, Yang Y, Li L, Tan Y, Chen Y, Wang S, et al. Pharmacokinetics and tissue distribution of trans-ferulic acid-4-β-glucoside in rats using UPLC-MS/MS. Biomed Chromatogr. 2022;36:e5327.
53. Luo Q, Xian P, Wang T, Wu S, Sun T, Wang W, et al. Antioxidant activity of mesenchymal stem cell-derived extracellular vesicles restores hippocampal neurons following seizure damage. Theranostics. 2021;11:5986–6005.
54. Yin Y, Gao D, Wang Y, Wang ZH, Wang X, Ye J, et al. Tau accumulation induces synaptic impairment and memory deficit by calcineurin-mediated inactivation of nuclear CaMKIV/CREB signaling. Proc Natl Acad Sci U S A. 2016;113:E3773–81.

55. Guo C, Liu Y, Fang MS, Li Y, Li W, Mahaman YAR, et al. omega-3PUFAs improve cognitive impairments through Ser133 phosphorylation of CREB upregulating BDNF/TrkB signal in Schizophrenia. Neurotherapeutics. 2020;17:1271–86.
56. Lesne S, Koh MT, Kotilinek L, Kayed R, Glabe CG, Yang A, et al. A specific amyloid-beta protein assembly in the brain impairs memory. Nature. 2006;440:352–7.
57. De Felice FG, Wu D, Lambert MP, Fernandez SJ, Velasco PT, Lacor PN, et al. Alzheimer's disease-type neuronal tau hyperphosphorylation induced by A beta oligomers. Neurobiol Aging. 2008;29:1334–47.
58. Nakazawa T, Komai S, Tezuka T, Hisatsune C, Umemori H, Semba K, et al. Characterization of Fyn-mediated tyrosine phosphorylation sites on GluR epsilon 2 (NR2B) subunit of the N-methyl-D-aspartate receptor. J Biol Chem. 2001;276:693–9.
59. Trepanier CH, Jackson MF, MacDonald JF. Regulation of NMDA receptors by the tyrosine kinase Fyn. FEBS J. 2012;279:12–9.
60. Paul S, Snyder GL, Yokakura H, Picciotto MR, Nairn AC, Lombroso PJ. The Dopamine/D1 receptor mediates the phosphorylation and inactivation of the protein tyrosine phosphatase STEP via a PKA-dependent pathway. J Neurosci. 2000;20:5630–8.
61. Valjent E, Pascoli V, Svenningsson P, Paul S, Enslen H, Corvol JC, et al. Regulation of a protein phosphatase cascade allows convergent dopamine and glutamate signals to activate ERK in the striatum. Proc Natl Acad Sci U S A. 2005;102:491–6.
62. Paul S, Nairn AC, Wang P, Lombroso PJ. NMDA-mediated activation of the tyrosine phosphatase STEP regulates the duration of ERK signaling. Nat Neurosci. 2003;6:34–42.
63. Reither G, Chatterjee J, Beullens M, Bollen M, Schultz C, Köhn M. Chemical activators of protein phosphatase-1 induce calcium release inside intact cells. Chem Biol. 2013;20:1179–86.
64. Serneels L, Van Biervliet J, Craessaerts K, Dejaegere T, Horré K, Van Houtvin T, et al. gamma-Secretase heterogeneity in the Aph1 subunit: relevance for Alzheimer's disease. Science. 2009;324:639–42.
65. Radde R, Bolmont T, Kaeser SA, Coomaraswamy J, Lindau D, Stoltze L, et al. Abeta42-driven cerebral amyloidosis in transgenic mice reveals early and robust pathology. EMBO Rep. 2006;7:940–6.
66. Maia LF, Kaeser SA, Reichwald J, Hruscha M, Martus P, Staufenbiel M, et al. Changes in amyloid-β and Tau in the cerebrospinal fluid of transgenic mice overexpressing amyloid precursor protein. Sci Transl Med. 2013;5:194re2.
67. Nativio R, Donahue G, Berson A, Lan Y, Amlie-Wolf A, Tuzer F, et al. Dysregulation of the epigenetic landscape of normal aging in Alzheimer's disease. Nat Neurosci. 2018;21:497–505.
68. Hardy JA, Higgins GA. Alzheimer's disease: the amyloid cascade hypothesis. Science. 1992;256:184–5.
69. Duyckaerts C, Delatour B, Potier MC. Classification and basic pathology of Alzheimer disease. Acta Neuropathol. 2009;118:5–36.
70. Selkoe DJ, Hardy J. The amyloid hypothesis of Alzheimer's disease at 25 years. EMBO Mol Med. 2016;8:595–608.
71. Jack CR Jr, Bennett DA, Blennow K, Carrillo MC, Dunn B, Haeberlein SB, et al. NIA-AA Research Framework: toward a biological definition of Alzheimer's disease. Alzheimers Dement. 2018;14:535–62.
72. Wang J, Gu BJ, Masters CL, Wang YJ. A systemic view of Alzheimer disease—insights from amyloid-β metabolism beyond the brain. Nat Rev Neurol. 2017;13:612–23.
73. Tu S, Okamoto S, Lipton SA, Xu H. Oligomeric Aβ-induced synaptic dysfunction in Alzheimer's disease. Mol Neurodegener. 2014;9:48.
74. Li Y, Rusinek H, Butler T, Glodzik L, Pirraglia E, Babich J, et al. Decreased CSF clearance and increased brain amyloid in Alzheimer's disease. Fluids Barriers CNS. 2022;19:21.
75. Mohamed LA, Qosa H, Kaddoumi A. Age-related decline in brain and hepatic clearance of amyloid-beta is rectified by the cholinesterase inhibitors donepezil and rivastigmine in rats. ACS Chem Neurosci. 2015;6:725–36.
76. Prasad H, Rao R. Amyloid clearance defect in ApoE4 astrocytes is reversed by epigenetic correction of endosomal pH. Proc Natl Acad Sci U S A. 2018;115:E6640–9.
77. Tian D-Y, Cheng Y, Zhuang Z-Q, He C-Y, Pan Q-G, Tang M-Z, et al. Physiological clearance of amyloid-beta by the kidney and its therapeutic potential for Alzheimer's disease. Mol Psychiatry. 2021;26:6074–82.
78. Xia Y, Wang ZH, Zhang Z, Liu X, Yu SP, Wang JZ, et al. Delta- and beta- secretases crosstalk amplifies the amyloidogenic pathway in Alzheimer's disease. Prog Neurobiol. 2021;204:102113.
79. Zhang Z, Li X-G, Wang Z-H, Song M, Yu SP, Kang SS, et al. δ-Secretase-cleaved Tau stimulates Aβ production via upregulating STAT1-BACE1 signaling in Alzheimer's disease. Mol Psychiatry. 2021;26:586–603.
80. Yao Y, Kang SS, Xia Y, Wang ZH, Liu X, Muller T, et al. A delta-secretase-truncated APP fragment activates CEBPB, mediating Alzheimer's disease pathologies. Brain. 2021;144:1833–52.
81. Zhang Z, Song M, Liu X, Su Kang S, Duong DM, Seyfried NT, et al. Delta-secretase cleaves amyloid precursor protein and regulates the pathogenesis in Alzheimer's disease. Nat Commun. 2015;6:8762.
82. Wu Z, Wang ZH, Liu X, Zhang Z, Gu X, Yu SP, et al. Traumatic brain injury triggers APP and Tau cleavage by delta-secretase, mediating Alzheimer's disease pathology. Prog Neurobiol. 2020;185:101730.
83. Zhang Z, Song M, Liu X, Kang SS, Kwon IS, Duong DM, et al. Cleavage of tau by asparagine endopeptidase mediates the neurofibrillary pathology in Alzheimer's disease. Nat Med. 2014;20:1254–62.
84. Chatterjee M, Kurup PK, Lundbye CJ, Hugger Toft AK, Kwon J, Benedict J, et al. STEP inhibition reverses behavioral, electrophysiologic, and synaptic abnormalities in Fmr1 KO mice. Neuropharmacology. 2018;128:43–53.
85. Kuchibhotla KV, Goldman ST, Lattarulo CR, Wu HY, Hyman BT, Bacskai BJ. Abeta plaques lead to aberrant regulation of calcium homeostasis in vivo resulting in structural and functional disruption of neuronal networks. Neuron. 2008;59:214–25.
86. Kuchibhotla KV, Lattarulo CR, Hyman BT, Bacskai BJ. Synchronous hyperactivity and intercellular calcium waves in astrocytes in Alzheimer mice. Science. 2009;323:1211–5.
87. Hu W, Wang Z, Zhang H, Mahaman YAR, Huang F, Meng D, et al. Chk1 inhibition ameliorates Alzheimer's disease pathogenesis and cognitive dysfunction through CIP2A/PP2A signaling. Neurotherapeutics. 2022.
88. Liu B, Kou J, Li F, Huo D, Xu J, Zhou X, et al. Lemon essential oil ameliorates age-associated cognitive dysfunction via modulating hippocampal synaptic density and inhibiting acetylcholinesterase. Aging (Albany NY). 2020;12:8622–39.
89. Szögi T, Schuster I, Borbély E, Gyebrovszki A, Bozsó Z, Gera J, et al. Effects of the pentapeptide P33 on memory and synaptic plasticity in APP/PS1 transgenic mice: a novel mechanism presenting the protein Fe65 as a target. Int J Mol Sci. 2019;20.
90. Alvarez A, Cacabelos R, Sanpedro C, Garcia-Fantini M, Aleixandre M. Serum TNF-alpha levels are increased and correlate negatively with free IGF-I in Alzheimer disease. Neurobiol Aging. 2007;28:533–6.
91. Pickering M, Cumiskey D, O'Connor JJ. Actions of TNF-alpha on glutamatergic synaptic transmission in the central nervous system. Exp Physiol. 2005;90:663–70.
92. Frankola KA, Greig NH, Luo W, Tweedie D. Targeting TNF-alpha to elucidate and ameliorate neuroinflammation in neurodegenerative diseases. CNS Neurol Disord Drug Targets. 2011;10:391–403.

93. Ransohoff RM. How neuroinflammation contributes to neurodegeneration. Science. 2016;353:777–83.
94. Heneka MT, Kummer MP, Stutz A, Delekate A, Schwartz S, Vieira-Saecker A, et al. NLRP3 is activated in Alzheimer's disease and contributes to pathology in APP/PS1 mice. Nature. 2013;493:674–8.
95. Calsolaro V, Edison P. Neuroinflammation in Alzheimer's disease: current evidence and future directions. Alzheimers Dement. 2016;12:719–32.
96. Busche MA, Hyman BT. Synergy between amyloid-β and tau in Alzheimer's disease. Nat Neurosci. 2020;23:1183–93.
97. Zhao J, Fu Y, Yamazaki Y, Ren Y, Davis MD, Liu C-C, et al. APOE4 exacerbates synapse loss and neurodegeneration in Alzheimer's disease patient iPSC-derived cerebral organoids. Nat Commun. 2020;11:5540.
98. Doody RS, Thomas RG, Farlow M, Iwatsubo T, Vellas B, Joffe S, et al. Phase 3 trials of solanezumab for mild-to-moderate Alzheimer's disease. N Engl J Med. 2014;370:311–21.
99. Ding XL, Lei P. Plasma replacement therapy for Alzheimer's disease. Neurosci Bull. 2020;36:89–90.
100. Floyd RA, Hensley K. Oxidative stress in brain aging. Implications for therapeutics of neurodegenerative diseases. Neurobiol Aging. 2002;23:795–807.
101. Salimi A, Li H, Lee JY. Molecular insight into the early stage of amyloid-β(1–42) Homodimers aggregation influenced by histidine tautomerism. Int J Biol Macromol. 2021;184:887–97.
102. Chiti F, Dobson CM. Protein misfolding, amyloid formation, and human disease: a summary of Progress over the last decade. Annu Rev Biochem. 2017;86:27–68.
103. Moon IS, Apperson ML, Kennedy MB. The major tyrosine-phosphorylated protein in the postsynaptic density fraction is N-methyl-D-aspartate receptor subunit 2B. Proc Natl Acad Sci U S A. 1994;91:3954–8.
104. Rostas JA, Brent VA, Voss K, Errington ML, Bliss TV, Gurd JW. Enhanced tyrosine phosphorylation of the 2B subunit of the N-methyl-D-aspartate receptor in long-term potentiation. Proc Natl Acad Sci U S A. 1996;93:10452–6.
105. Lussier MP, Sanz-Clemente A, Roche KW. Dynamic regulation of N-methyl-d-aspartate (NMDA) and α-amino-3-hydroxy-5-methyl-4-isoxazolepropionic acid (AMPA) receptors by post-translational modifications. J Biol Chem. 2015;290:28596–603.
106. Furukawa H, Singh SK, Mancusso R, Gouaux E. Subunit arrangement and function in NMDA receptors. Nature. 2005;438:185–92.
107. Barria A, Malinow R. Subunit-specific NMDA receptor trafficking to synapses. Neuron. 2002;35:345–53.
108. Zhang L, Xie JW, Yang J, Cao YP. Tyrosine phosphatase STEP61 negatively regulates amyloid β-mediated ERK/CREB signaling pathways via α7 nicotinic acetylcholine receptors. J Neurosci Res. 2013;91:1581–90.
109. Chin J, Palop JJ, Puoliväli J, Massaro C, Bien-Ly N, Gerstein H, et al. Fyn kinase induces synaptic and cognitive impairments in a transgenic mouse model of Alzheimer's disease. J Neurosci. 2005;25:9694–703.
110. Nguyen TH, Liu J, Lombroso PJ. Striatal enriched phosphatase 61 dephosphorylates Fyn at phosphotyrosine 420. J Biol Chem. 2002;277:24274–9.
111. Dohadwala M, da Cruz e Silva EF, Hall FL, Williams RT, Carbonaro-Hall DA, Nairn AC, et al. Phosphorylation and inactivation of protein phosphatase 1 by cyclin-dependent kinases. Proc Natl Acad Sci U S A. 1994;91:6408–12.
112. Hou H, Sun L, Siddoway BA, Petralia RS, Yang H, Gu H, et al. Synaptic NMDA receptor stimulation activates PP1 by inhibiting its phosphorylation by Cdk5. J Cell Biol. 2013;203:521–35.
113. Roberts TF, Tschida KA, Klein ME, Mooney R. Rapid spine stabilization and synaptic enhancement at the onset of behavioural learning. Nature. 2010;463:948–52.
114. El-Husseini AE, Schnell E, Chetkovich DM, Nicoll RA, Bredt DS. PSD-95 involvement in maturation of excitatory synapses. Science. 2000;290:1364–8.
115. Yu W, Lu B. Synapses and dendritic spines as pathogenic targets in Alzheimer's disease. Neural Plast. 2012;2012:247150.
116. Skaper SD, Facci L, Zusso M, Giusti P. Synaptic plasticity, dementia and Alzheimer disease. CNS Neurol Disord Drug Targets. 2017;16:220–33.
117. Zhu J, Shang Y, Zhang M. Mechanistic basis of MAGUK-organized complexes in synaptic development and signalling. Nat Rev Neurosci. 2016;17:209–23.
118. Omelchenko A, Menon H, Donofrio SG, Kumar G, Chapman HM, Roshal J, et al. Interaction between CRIPT and PSD-95 is required for proper dendritic arborization in hippocampal neurons. Mol Neurobiol. 2020;57:2479–93.
119. Wang W, Weng J, Zhang X, Liu M, Zhang M. Creating conformational entropy by increasing interdomain mobility in ligand binding regulation: a revisit to N-terminal tandem PDZ domains of PSD-95. J Am Chem Soc. 2009;131:787–96.
120. Sheng N, Bemben MA, Díaz-Alonso J, Tao W, Shi YS, Nicoll RA. LTP requires postsynaptic PDZ-domain interactions with glutamate receptor/auxiliary protein complexes. Proc Natl Acad Sci U S A. 2018;115:3948–53.
121. Chen X, Levy JM, Hou A, Winters C, Azzam R, Sousa AA, et al. PSD-95 family MAGUKs are essential for anchoring AMPA and NMDA receptor complexes at the postsynaptic density. Proc Natl Acad Sci U S A. 2015;112:E6983–92.
122. Gardoni F, Bellone C, Viviani B, Marinovich M, Meli E, Pellegrini-Giampietro DE, et al. Lack of PSD-95 drives hippocampal neuronal cell death through activation of an alpha CaMKII transduction pathway. Eur J Neurosci. 2002;16:777–86.
123. Zhang J, Xu TX, Hallett PJ, Watanabe M, Grant SG, Isacson O, et al. PSD-95 uncouples dopamine-glutamate interaction in the D1/PSD-95/NMDA receptor complex. J Neurosci. 2009;29:2948–60.
124. Dore K, Carrico Z, Alfonso S, Marino M, Koymans K, Kessels HW, et al. PSD-95 protects synapses from β-amyloid. Cell Rep. 2021;35:109194.
125. Ugalde-Triviño L, Díaz-Guerra M. PSD-95: an effective target for stroke therapy using neuroprotective peptides. Int J Mol Sci. 2021;22:12585.
126. Cesca F, Baldelli P, Valtorta F, Benfenati F. The synapsins: key actors of synapse function and plasticity. Prog Neurobiol. 2010;91:313–48.
127. Helm MS, Dankovich TM, Mandad S, Rammner B, Jähne S, Salimi V, et al. A large-scale nanoscopy and biochemistry analysis of postsynaptic dendritic spines. Nat Neurosci. 2021;24:1151–62.
128. Yan JJ, Jung JS, Kim TK, Hasan A, Hong CW, Nam JS, et al. Protective effects of ferulic acid in amyloid precursor protein plus presenilin-1 transgenic mouse model of Alzheimer disease. Biol Pharm Bull. 2013;36:140–3.
129. Kang SS, Ahn EH, Zhang Z, Liu X, Manfredsson FP, Sandoval IM, et al. α-Synuclein stimulation of monoamine oxidase-B and legumain protease mediates the pathology of Parkinson's disease. EMBO J. 2018;37.
130. Kang SS, Liu X, Ahn EH, Xiang J, Manfredsson FP, Yang X, et al. Norepinephrine metabolite DOPEGAL activates AEP and pathological Tau aggregation in locus coeruleus. J Clin Invest. 2020;130:422–37.
131. Iwata N, Tsubuki S, Takaki Y, Watanabe K, Sekiguchi M, Hosoki E, et al. Identification of the major Aβ1-42-degrading catabolic pathway in brain parenchyma: suppression leads to biochemical and pathological deposition. Nat Med. 2000;6:143–50.
132. Leite JP, Lete MG, Fowler SB, Gimeno A, Rocha JF, Sousa SF, et al. Aβ(31–35) Decreases neprilysin-mediated Alzheimer's amyloid-β peptide degradation. ACS Chem Neurosci. 2021;12:3708–18.

133. Stargardt A, Gillis J, Kamphuis W, Wiemhoefer A, Kooijman L, Raspe M, et al. Reduced amyloid-β degradation in early Alzheimer's disease but not in the APPswePS1dE9 and 3xTg-AD mouse models. Aging Cell. 2013;12:499–507.
134. Kurochkin IV, Guarnera E, Berezovsky IN. Insulin-degrading enzyme in the fight against Alzheimer's disease. Trends Pharmacol Sci. 2018;39:49–58.
135. Farris W, Mansourian S, Chang Y, Lindsley L, Eckman EA, Frosch MP, et al. Insulin-degrading enzyme regulates the levels of insulin, amyloid beta-protein, and the beta-amyloid precursor protein intracellular domain in vivo. Proc Natl Acad Sci U S A. 2003;100:4162–7.
136. Vepsäläinen S, Helisalmi S, Mannermaa A, Pirttilä T, Soininen H, Hiltunen M. Combined risk effects of IDE and NEP gene variants on Alzheimer disease. J Neurol Neurosurg Psychiatry. 2009;80:1268–70.
137. Chen S, Mima D, Jin H, Dan Q, Wang F, Cai J, et al. The association between Neprilysin gene polymorphisms and Alzheimer's disease in Tibetan population. Brain Behav. 2021;11:e02002.
138. Dorfman VB, Pasquini L, Riudavets M, López-Costa JJ, Villegas A, Troncoso JC, et al. Differential cerebral deposition of IDE and NEP in sporadic and familial Alzheimer's disease. Neurobiol Aging. 2010;31:1743–57.
139. Shibata M, Yamada S, Kumar SR, Calero M, Bading J, Frangione B, et al. Clearance of Alzheimer's amyloid-ss(1–40) peptide from brain by LDL receptor-related protein-1 at the blood-brain barrier. J Clin Invest. 2000;106:1489–99.
140. Kang DE, Pietrzik CU, Baum L, Chevallier N, Merriam DE, Kounnas MZ, et al. Modulation of amyloid beta-protein clearance and Alzheimer's disease susceptibility by the LDL receptor-related protein pathway. J Clin Invest. 2000;106:1159–66.
141. Halliday MR, Rege SV, Ma Q, Zhao Z, Miller CA, Winkler EA, et al. Accelerated pericyte degeneration and blood-brain barrier breakdown in apolipoprotein E4 carriers with Alzheimer's disease. J Cereb Blood Flow Metab. 2016;36:216–27.
142. Ma Q, Zhao Z, Sagare AP, Wu Y, Wang M, Owens NC, et al. Blood-brain barrier-associated pericytes internalize and clear aggregated amyloid-β42 by LRP1-dependent apolipoprotein E isoform-specific mechanism. Mol Neurodegener. 2018;13:57.
143. Storck SE, Meister S, Nahrath J, Meißner JN, Schubert N, Di Spiezio A, et al. Endothelial LRP1 transports amyloid-β(1–42) across the blood-brain barrier. J Clin Invest. 2016;126:123–36.
144. Nikolakopoulou AM, Wang Y, Ma Q, Sagare AP, Montagne A, Huuskonen MT, et al. Endothelial LRP1 protects against neurodegeneration by blocking cyclophilin A. J Exp Med. 2021;218.
145. Heneka MT, Golenbock DT, Latz E. Innate immunity in Alzheimer's disease. Nat Immunol. 2015;16:229–36.
146. Leng F, Edison P. Neuroinflammation and microglial activation in Alzheimer disease: where do we go from here? Nat Rev Neurol. 2021;17:157–72.
147. Castillo E, Leon J, Mazzei G, Abolhassani N, Haruyama N, Saito T, et al. Author Correction: Comparative profiling of cortical gene expression in Alzheimer's disease patients and mouse models demonstrates a link between amyloidosis and neuroinflammation. Sci Rep. 2021;11:18377.
148. Kou J-j, Shi J-z, He Y-y, Hao J-j, Zhang H-y, Luo D-m, et al. Luteolin alleviates cognitive impairment in Alzheimer's disease mouse model via inhibiting endoplasmic reticulum stress-dependent neuroinflammation. Acta Pharmacol Sin. 2021;43:840–9.
149. Hur J-Y, Frost GR, Wu X, Crump C, Pan SJ, Wong E, et al. The innate immunity protein IFITM3 modulates γ-secretase in Alzheimer's disease. Nature. 2020;586:735–40.
150. Katsuki H, Nakai S, Hirai Y, Akaji K, Kiso Y, Satoh M. Interleukin-1 beta inhibits long-term potentiation in the CA3 region of mouse hippocampal slices. Eur J Pharmacol. 1990;181:323–6.
151. Bains JS, Oliet SH. Glia: they make your memories stick! Trends Neurosci. 2007;30:417–24.
152. Beattie EC, Stellwagen D, Morishita W, Bresnahan JC, Ha BK, Von Zastrow M, et al. Control of synaptic strength by glial TNFalpha. Science. 2002;295:2282–5.
153. Sultana R, Ravagna A, Mohmmad-Abdul H, Calabrese V, Butterfield DA. Ferulic acid ethyl ester protects neurons against amyloid beta- peptide(1–42)-induced oxidative stress and neurotoxicity: relationship to antioxidant activity. J Neurochem. 2005;92:749–58.
154. Lok K, Zhao H, Shen H, Wang Z, Gao X, Zhao W, et al. Characterization of the APP/PS1 mouse model of Alzheimer's disease in senescence accelerated background. Neurosci Lett. 2013;557:84–9.
155. Kim HS, Cho JY, Kim DH, Yan JJ, Lee HK, Suh HW, et al. Inhibitory effects of long-term administration of ferulic acid on microglial activation induced by intracerebroventricular injection of beta-amyloid peptide (1–42) in mice. Biol Pharm Bull. 2004;27:120–1.